NONLOCAL HYBRID-KINETIC STABILITY ANALYSIS OF THE DRIFT-CONE INSTABILITY

Ronald C. Davidson and Han S. Uhm*
Plasma Fusion Center, M.I.T.
Cambridge, Massachusetts 02139

Richard E. Aamodt
Science Applications, Inc.
934 Pearl St., Boulder, Colorado 80302

PFC/JA-79-3

Submitted to Physics of Fluids,
February 1979

* Also at Naval Surface Weapons Center, Silver Spring, Md. 20910.

NONLOCAL HYBRID-KINETIC STABILITY ANALYSIS OF THE MIRROR DRIFT-CONE INSTABILITY

Ronald C. Davidson and Han S. Uhm*
Plasma Fusion Center, Massachusetts Institute of Technology
Cambridge, Massachusetts 02139

Richard E. Aamodt
Science Applications, Inc.,
934 Pearl St., Boulder, Colorado 80302

ABSTRACT

A hybrid-kinetic model (Vlasov ions and cold-fluid electrons) is used to develop a fully nonlocal theory of the mirror-drift-cone instability. The stability analysis assumes electrostatic flute perturbations about a cylindrical ion equilibrium $f_i^0(H_1-\omega_i P_\theta, v_z)$, where ω_i= const.=angular velocity of mean rotation. The radial eigenvalue equation for the potential amplitude $\hat{\phi}(r)$ is solved exactly for the particular choice of f_i^0 corresponding to a sharp-boundary (rectangular) density profile. The resulting dispersion relation for the complex eigenfrequency ω is investigated numerically for a broad range of system parameters including the important influence of large ion orbits and ion thermal effects. It is found that the instability growth rate is typically more severe for fast rotational equilibria ($\omega_i=\hat{\omega}_i^+$) with axis encircling orbits than for slow rotational equilibria ($\omega_i=\hat{\omega}_i^-$). Stability behavior is investigated for the entire range of $\hat{r}_{Li}/R_p$ allowed by the equilibrium model ($0<2\hat{r}_{Li}/R_p<1$).

*Also at Naval Surface Weapons Center, Silver Spring, Md. 20910

I. INTRODUCTION

One of the most basic instabilities that characterizes a mirror-confined plasma is the mirror drift-cone instability.[1-3] In cylindrical geometry (Fig. 1), the instability results from the relative mean azimuthal motion between ions and electrons in the presence of spatial inhomogeneities. Conventional theories of this instability for both weak-gradient[1,2] and strong-gradient[3] configurations are usually based on the local approximation,[4] which assumes short azimuthal wavelengths and that the radial eigenfunction is localized over a radial distance much shorter than the characteristic inhomogeneity length. The purpose of this paper is to develop a fully self-consistent nonlocal theory of the mirror-drift-cone instability with emphasis on the influence of large ion Larmor radius and axis-encircling orbits[5] on stability behavior.

The analysis is carried out within the framework of a hybrid Vlasov-fluid model. The electrons are described as a macroscopic, cold ($T_e \to 0$) fluid immersed in a uniform axial magnetic field $B_0\hat{e}_z$. On the other hand, we adopt a fully kinetic model for the ions in which the ions are described by the Vlasov equation. This allows for the possibility of large ion orbits with characteristic thermal Larmor radius ($\hat{r}_{Li}$) comparable to the radius of the plasma column (R_p). Such hybrid models have also proven quite tractable for nonneutral plasma,[6,7] theta-pinch,[8] and ion-layer[9] applications. Indeed, the present analysis of the mirror drift-cone instability closely parallels the nonlocal formalism developed by Davidson and Uhm[6] for investigation of the ion resonance instability in a

nonneutral plasma column. Therefore, the description of the theoretical model in Secs. II and III is appropriately brief.

The outline of this paper is the following. In Sec. II, we describe the hybrid Vlasov-fluid model (Sec. II.A) and summarize the equilibrium formalism (Sec. II.B) for ion distribution functions of the form

$$f_i^0(\underset{\sim}{x},\underset{\sim}{v})=f_i^0(H_\perp-\omega_i P_\theta, v_z) \ ,$$

where v_z is the axial velocity, $H_\perp$ is the perpendicular kinetic energy, P_θ is the canonical angular momentum, and ω_i=const. is the angular velocity of mean rotation. The analysis assumes equilibrium charge neutrality [Eq. (5)] with

$$n_e^0(r)=n_i^0(r)$$

and zero equilibrium radial electric field, i.e., $E_r^0(r)=0$. In Sec. II.C, equilibrium properties are calculated for the case where the ion and electron density profiles are rectangular (Fig. 2) and the ion distribution function is specified by [Eq. (10)]

$$f_i^0(\underset{\sim}{x},\underset{\sim}{v}) = \frac{n_0 m_i}{2\pi}\,\delta(H_\perp-\omega_i P_\theta-\hat{T}_i)G(v_z) \ ,$$

where n_0 and $\hat{T}_i$ are positive constants. Electrostatic stability properties are calculated in Secs. III and IV, assuming flute perturbations ($\partial/\partial z$=0) about a cylindrically symmetric equilibrium. The general eigenvalue equation [Eq. (16)] is formulated in Sec. III.A for arbitrary $f_i^0(H_\perp-\omega_i P_\theta,\ v_z)$. In Secs. III.B and III.C, assuming rectangular ion and electron density profiles and f_i^0 specified by Eq. (10), the eigenvalue equation (16) is then solved in circum-

stances where the perturbed charge density corresponds to a surface-charge perturbation (at $r=R_p$). A remarkable feature of this analysis is the fact that the required orbit integral $\hat{I}$ [Eq. (17)] can be evaluated in closed form [Eqs. (18) and (20)] for general values of the parameters $\hat{r}_{Li}/R_p$, $\hat{\omega}_{pi}^2/\omega_{ci}^2$, etc. Moreover, the resulting eigenvalue equation (19) for the perturbed potential $\hat{\phi}_\ell(r)$ can be solved exactly to give a closed algebraic dispersion relation (24) for the complex eigenfrequency ω.

The general dispersion relation (24) is an algebraic equation of order $\ell+2$, where ℓ is the azimuthal mode number. In Sec. IV, a detailed numerical analysis of Eq. (24) is presented for a broad range of system parameters. It is found that the growth rate of the mirror drift-cone instability exhibits a sensitive dependence on $\hat{r}_{Li}/R_p$, R_p/R_c, etc. Moreover, the instability growth rate is typically more severe when the ions are in a fast rotational equilibrium ($\omega_i=\hat{\omega}_i^+$) rather than a slow rotational equilibrium ($\omega_i=\hat{\omega}_i^-$). The reason is simply that the relative drift between the ions and electrons is larger ($|\hat{\omega}_i^+|>|\hat{\omega}_i^-|$), and hence more free energy is available to drive the instability. [See also Eq. (13) and Fig. 3.]

In conclusion, we emphasize that the present sharp-boundary calculation of the mirror-drift-cone instability represents a "worst-case" stability analysis. The stability behavior for diffuse equilibrium profiles is currently under investigation, making use of the hybrid-kinetic eigenvalue equation (16) derived for general $f_i^0(H_\perp-\omega_i P_\theta, v_z)$.

II. THEORETICAL MODEL AND EQUILIBRIUM PROPERTIES

A. Theoretical Model

The present analysis is carried out within the framework of a hybrid Vlasov-fluid model in which the electrons are described as a macroscopic, cold ($T_e \to 0$) fluid immersed in a uniform axial magnetic field $B_0\hat{e}_z$, and the ions are described by the Vlasov equation. Within the context of the electrostatic approximation ($\underset{\sim}{B} \simeq B_0\hat{e}_z$ and $\nabla \times \underset{\sim}{E} = 0$), the equation of motion and continuity equation for the electron fluid can be expressed as

$$\left(\frac{\partial}{\partial t} + \underset{\sim}{V}_e \cdot \frac{\partial}{\partial \underset{\sim}{x}}\right) \underset{\sim}{V}_e = -\frac{e}{m_e}\left(-\nabla\phi + \frac{\underset{\sim}{V}_e \times B_0\hat{e}_z}{c}\right), \qquad (1)$$

$$\left(\frac{\partial}{\partial t} + \underset{\sim}{V}_e \cdot \frac{\partial}{\partial \underset{\sim}{x}}\right) n_e = -n_e \frac{\partial}{\partial \underset{\sim}{x}} \cdot \underset{\sim}{V}_e , \qquad (2)$$

where $\underset{\sim}{E}(\underset{\sim}{x},t) = -\nabla\phi(\underset{\sim}{x},t)$ is the electric field, $n_e(\underset{\sim}{x},t)$ is the electron density, $\underset{\sim}{V}_e(\underset{\sim}{x},t)$ is the mean electron velocity, and $-e$ and m_e are the electron charge and mass, respectively. In Eq. (1), the spatial variation in B_0 is neglected (low-beta approximation). To allow for the possibility of large ion orbits with thermal Larmor radius comparable to the radius of the plasma column, we adopt a fully kinetic model in which the ion distribution function $f_i(\underset{\sim}{x},\underset{\sim}{v},t)$ evolves according to the Vlasov equation

$$\left[\frac{\partial}{\partial t} + \underset{\sim}{v} \cdot \frac{\partial}{\partial \underset{\sim}{x}} + \frac{e}{m_i}\left(-\nabla\phi + \frac{\underset{\sim}{v} \times B_0\hat{e}_z}{c}\right) \cdot \frac{\partial}{\partial \underset{\sim}{v}}\right] f_i(\underset{\sim}{x},\underset{\sim}{v},t) = 0, \qquad (3)$$

where $+e$ and m_i are the ion charge and mass, respectively, and the electrostatic potential in Eqs. (1) and (3) is determined self-consistently from Poisson's equation

$$\nabla^2\phi = -4\pi e\left(\int d^3v\, f_i - n_e\right) . \qquad (4)$$

Equations (1)-(4) constitute a closed description of equilibrium and stability properties, and form the theoretical basis for the subsequent analysis.

B. General Equilibrium Properties

An equilibrium analysis of Eqs. (1)-(4) for general steady-state ($\partial/\partial t=0$) profiles proceeds in the following manner. We consider an infinitely long plasma column with equilibrium properties characterized by $\partial/\partial\theta=0=\partial/\partial z$. Here, cylindrical polar coordinates (r,θ,z) have been introduced, where the z-axis coincides with the axis of symmetry, r is the radial distance from the z-axis, and θ is the polar angle [Fig. 1]. For cylindrically symmetric electron equilibria described by $n_e^0(r)$ and $\underset{\sim}{V}_e^0(\underset{\sim}{x})=V_{e\theta}^0(r)\hat{\underset{\sim}{e}}_\theta$, it is straightforward to show from Eq. (2) that the functional form of the electron density profile $n_e^0(r)$ can be specified arbitrarily. For present purposes, it is assumed that $n_e^0(r)$ corresponds to equilibrium charge neutrality, i.e., we choose

$$n_e^0(r)=n_i^0(r) \ , \tag{5}$$

where $n_i^0(r)$ is the equilibrium ion density profile calculated from $n_i^0(r)=\int d^3v\ f_i^0$. Consistent with Eq. (5) and the steady-state ($\partial/\partial t=0$) versions of Eqs. (1) and (4), it is also assumed that the equilibrium radial electric field is equal to zero, i.e., $E_r^0(r)=-\partial\phi^0/\partial r=0$, and that the equilibrium electron motion is stationary, with $V_{e\theta}^0(r)=\omega_e(r)r=0$.

For the ions, any distribution function $f_i^0(\underset{\sim}{x},\underset{\sim}{v})$ that is a function of the single-particle constants of the motion in the equilibrium fields is a solution to the steady-state ($\partial/\partial t=0$) ion Vlasov equation. For present purposes, we consider the class

of rigid-rotor ion Vlasov equilibria described by[6,7,10]

$$f_i^0=f_i^0(H_\perp-\omega_i P_\theta,v_z) \ , \tag{6}$$

where ω_i=const., v_z is the axial velocity, $H_\perp=(m_i/2)(v_r^2+v_\theta^2)$ is the perpendicular energy (with $\phi^0=0$), $P_\theta=m_i r(v_\theta+r\omega_{ci}/2)$ is the canonical angular momentum, and $\omega_{ci}=eB_0/m_i c$ is the ion cyclotron frequency. An important feature of Eq. (6) is that the mean azimuthal motion corresponds to a rigid rotation with angular velocity ω_i=const. Defining the mean azimuthal velocity by $V_{i\theta}^0(r)=(\int d^3v\ v_\theta\ f_i^0)/(\int d^3v\ f_i^0)$, it is straightforward to show that $V_{i\theta}^0(r)=\omega_i r$ for the class of ion equilibria described by Eq. (6). In the equilibrium and stability analysis that follows, it is useful to introduce perpendicular velocity variables appropriate to the rotating frame of the ions. Defining $V_x=v_x+\omega_i y$ and $V_y=v_y-\omega_i x$ (or equivalently $V_r=v_r$ and $V_\theta=v_\theta-\omega_i r$), we find

$$H_\perp-\omega_i P_\theta=(m_i/2)V_\perp^2+\psi(r) \ , \tag{7}$$

where $V_\perp^2=V_x^2+V_y^2=V_r^2+V_\theta^2$, and $\psi(r)$ is defined by

$$\psi(r)=(m_i/2)\Omega^2 r^2 \ ,$$

where $\Omega^2=-\omega_i(\omega_i+\omega_{ci})>0$ by assumption. Note in Eq. (7) that $m_i V_\perp^2/2$ is the perpendicular ion kinetic energy in a frame of reference rotating with angular velocity ω_i, and $\psi(r)$ is the effective potential in the rotating frame. Substituting Eq. (7) into Eq. (6), the equilibrium ion density profile $n_i^0(r)=\int d^3v\ f_i^0$ can be expressed as

$$n_i^0(r)=\int d^3V\ f_i^0\left(\frac{m_i}{2}\ V_\perp^2+\psi(r),\ v_z\right) \tag{8}$$

where $\int d^3V = 2\pi \int_0^\infty dV_\perp V_\perp \int_{-\infty}^\infty dv_z$. Moreover, it can also be shown that the equilibrium pressure tensor in a plane perpendicular to $\hat{e}_z$ is isotropic with perpendicular pressure $P_{i\perp}^0(r) = n_i^0(r) T_{i\perp}^0(r)$ given by

$$n_i^0(r) T_{i\perp}^0(r) = \int d^3V \frac{m_i}{2} V_\perp^2 f_i^0 \left(\frac{m_i}{2} V_\perp^2 + \psi(r), v_z \right) . \tag{9}$$

Equation (9), in effect, determines the perpendicular ion temperature profile $T_{i\perp}^0(r)$ in terms of f_i^0.

C. Sharp-Boundary Equilibrium

As a simple equilibrium example that gives a rectangular density profile, we consider the ion equilibrium specified by

$$f_i^0 = (n_0 m_i / 2\pi) \delta(H_\perp - \omega_i P_\theta - \hat{T}_i) G(v_z) , \tag{10}$$

where n_0 and $\hat{T}_i$ are positive constants, and $G(v_z)$ has normalization $\int_{-\infty}^\infty dv_z G(v_z) = 1$. Substituting Eq. (10) into Eq. (8) readily gives the sharp-boundary density profile

$$n_i^0(r) = \begin{cases} n_0 = \text{const.}, & r < R_p , \\ 0 , & r > R_p , \end{cases} \tag{11}$$

where the column radius R_p is determined self-consistently from $\psi(R_p) = (m_i/2)\Omega^2 R_p^2 = \hat{T}_i$, or equivalently $R_p^2 = (2\hat{T}_i / m_i \Omega^2)$, where $\Omega^2 = -\omega_i(\omega_i + \omega_{ci}) > 0$. The electron density profile $n_e^0(r)$ is assumed to have the same form as in Eq. (11) [see Eq. (5)]. We make use of Eqs. (9)-(11) to determine the perpendicular ion temperature $T_{i\perp}^0(r)$. This gives the parabolic profile

$$T_{i\perp}^0(r) = \hat{T}_i (1 - r^2/R_p^2) \tag{12}$$

for $0 < r < R_p$. The equilibrium profiles in Eqs. (11) and (12) are

illustrated in Fig. 2.

For future reference, it is useful to introduce the ion diamagnetic frequency defined by $\omega_{di}=(c/eB_0n_i^0r)(\partial/\partial r)(n_i^0T_{i\perp}^0)$. Making use of Eqs. (11) and (12) gives the constant value $\omega_{di}=-(\hat{T}_ic/eB_0)(2/R_p^2)=$ const. Moreover, making use of $R_p^2=-2\hat{T}_i/m_i\omega_i(\omega_i+\omega_{ci})$ gives the identity

$$\omega_i^2+\omega_i\omega_{ci}=\omega_{ci}\omega_{di} ,$$

which is simply a statement of radial force balance (of centrifugal, magnetic, and pressure gradient forces) on an ion fluid element for choice of equilibrium distribution function in Eq. (10). For specified values of R_p and $\hat{T}_i$ (and hence ω_{di}), the relation $\omega_i^2+\omega_i\omega_{ci}=\omega_{ci}\omega_{di}$ can be used to determine the rotation velocity ω_i. We find that both slow ($\hat{\omega}_i^-$) and fast ($\hat{\omega}_i^+$) rotational solutions exist with

$$\omega_i=\hat{\omega}_i^{\pm}= -\frac{\omega_{ci}}{2}\left[1\pm\left(1-4\frac{\hat{r}_{Li}^2}{R_p^2}\right)^{1/2}\right] . \qquad (13)$$

In Eq. (15), $\hat{r}_{Li}=(2\hat{T}_i/m_i\omega_{ci}^2)^{1/2}=(-\omega_{di}R_p^2/\omega_{ci})^{1/2}$ is the thermal ion Larmor radius associated with the on-axis (r=0) ion temperature $\hat{T}_i$. Note from Eq. (13) that equilibrium solutions exist only for $2\hat{r}_{Li}<R_p$ for the choice of ion distribution function in Eq. (10). Figure 3 shows a plot of $\hat{\omega}_i^{\pm}$ versus $4\hat{r}_{Li}^2/R_p^2$ for the allowed range $0<4\hat{r}_{Li}^2/R_p^2<1$. Evidently, for $4\hat{r}_{Li}^2<<R_p^2$, the slow rotational equilibrium ($\omega_i=\hat{\omega}_i^-$) corresponds to a rotation at the ion diamagnetic frequency with $\omega_i\simeq\omega_{di}=-\omega_{ci}\hat{r}_{Li}^2/R_p^2$. Moreover, $\omega_i=\hat{\omega}_i^+$ corresponds to a fast rotational equilibrium with axis-encircling orbits.

For use in the subsequent stability analysis, we record here the ion trajectory $\underset{\sim}{x}'(t')$ that satisfies $d\underset{\sim}{x}'(t')/dt'=\underset{\sim}{v}'(t')$ and $d\underset{\sim}{v}'(t')/dt'=(e/m_ic)\underset{\sim}{v}'(t')\times B_0\hat{\underset{\sim}{e}}_z$, subject to the "initial" conditions

$\underset{\sim}{x}'(t'=t)=\underset{\sim}{x}$ and $\underset{\sim}{y}'(t'=t)=\underset{\sim}{y}$. In terms of the rotating frame variables $(v_x+\omega_i y,\ v_y-\omega_i x)=(V_x,V_y)=(V_\perp\cos\phi,\ V_\perp\sin\phi)$ and $(x,y)=(r\cos\theta,\ r\sin\theta)$, it is readily shown that

$$x'(\tau)=-\omega_{ci}^{-1}\{V_\perp[\sin(\phi-\omega_{ci}\tau)-\sin\phi] + r\omega_i\cos(\theta-\omega_{ci}\tau)-r(\omega_i+\omega_{ci})\cos\theta\}\ ,$$

$$y'(\tau)=-\omega_{ci}^{-1}\{V_\perp[\cos\phi-\cos(\phi-\omega_{ci}\tau)] + r\omega_i\sin(\theta-\omega_{ci}\tau)-r(\omega_i+\omega_{ci})\sin\theta\}\ , \qquad (14)$$

where $\tau=t'-t$, and $\omega_i=\hat{\omega}_i^-$ for a slow rotational equilibrium, or $\omega_i=\hat{\omega}_i^+$ for a fast rotational equilibrium.

III. ELECTROSTATIC STABILITY PROPERTIES

A. General Eigenvalue Equation

In this section, we linearize Eqs. (1)-(4) assuming electrostatic perturbations about the general class of axisymmetric equilibria described by ion distribution function $f_i^0=f_i^0(H_\perp-\omega_i P_\theta,v_z)$ [Eq. (6)] and electron density profile $n_e^0(r)=n_i^0(r)$ [Eq. (5)]. The present analysis assumes flute perturbations with $\partial/\partial z=0$, so that all perturbations have spatial dependence only on $\underset{\sim}{x}_\perp=(x,y)$, or equivalently $\underset{\sim}{x}_\perp=(r,\theta)$. In the electrostatic approximation the perturbed electric field is $\delta\underset{\sim}{E}(\underset{\sim}{x}_\perp,t)=-\nabla_\perp\delta\phi(\underset{\sim}{x}_\perp,t)$. Substituting $\delta\phi(\underset{\sim}{x}_\perp,t)=\delta\hat{\phi}(\underset{\sim}{x}_\perp)\exp(-i\omega t)$ (with $\mathrm{Im}\omega>0$) in the linearized version of Eq. (3), the perturbed ion distribution function[6] can be expressed as $\delta f_i(\underset{\sim}{x},\underset{\sim}{v},t)=\delta\hat{f}_i(\underset{\sim}{x}_\perp,\underset{\sim}{v})\exp(-i\omega t)$, where

$$\delta\hat{f}_i(\underset{\sim}{x}_\perp,\underset{\sim}{v})=e\frac{\partial f_i^0}{\partial H_\perp}\left(\delta\hat{\phi}(\underset{\sim}{x}_\perp)+\int_{-\infty}^{0}d\tau\exp(-i\omega\tau)(i\omega-\omega_i\frac{\partial}{\partial\theta'})\delta\hat{\phi}(\underset{\sim}{x}_\perp')\right) . \tag{15}$$

In Eq. (15), $\underset{\sim}{x}_\perp'(t')=[x'(t'),y'(t')]$ is the ion trajectory defined in Eq. (14), and use has been made of $\partial f_i^0/\partial P_\theta=-\omega_i\partial f_i^0/\partial H_\perp$ for the class of ion equilibria with $f_i^0=f_i^0(H_\perp-\omega_i P_\theta,v_z)$. We consider perturbations of the form $\delta\hat{\phi}(\underset{\sim}{x}_\perp)=\hat{\phi}_\ell(r)\exp(i\ell\theta)$, $\delta\hat{n}_e(\underset{\sim}{x}_\perp)=\hat{n}_{e\ell}(r)\exp(i\ell\theta)$, etc., where ℓ is the azimuthal harmonic number. After some straightforward algebra[6] that makes use of the linearized versions of Eqs. (1) and (2), the perturbed electron density $\hat{n}_{e\ell}(r)$ can be expressed directly in terms of the potential amplitude $\hat{\phi}_\ell(r)$. Then, making use of Eq. (4) with $\delta\hat{f}_i(\underset{\sim}{x}_\perp,\underset{\sim}{v})$ specified by Eq. (15), the linearized Poisson

equation for $\hat{\phi}(r)=\hat{\phi}_\ell(r)$ can be expressed as

$$\frac{1}{r}\frac{\partial}{\partial r}\left[r\left(1-\frac{\omega_{pe}^2}{\omega^2-\omega_{ce}^2}\right)\frac{\partial}{\partial r}\hat{\phi}(r)\right]-\frac{\ell^2}{r^2}\left(1-\frac{\omega_{pe}^2}{\omega^2-\omega_{ce}^2}\right)\hat{\phi}(r)$$

$$=\frac{\ell\hat{\phi}(r)}{r}\frac{\omega_{ce}}{\omega(\omega^2-\omega_{ce}^2)}\frac{\partial}{\partial r}\omega_{pe}^2(r) \qquad (16)$$

$$-\frac{4\pi e^2}{m_i}\int d^3V\,\frac{1}{V_\perp}\frac{\partial f_i^0}{\partial V_\perp}\left[\hat{\phi}(r)+(\omega-\ell\omega_i)\hat{I}\right] \quad ,$$

where $\omega_{pe}^2(r)=4\pi n_e^0(r)e^2/m_e$, $\int d^3V=2\pi\int_0^\infty dV_\perp V_\perp\int_{-\infty}^\infty dv_z$, and use has been made of $\partial f_i^0/\partial H_\perp=(m_iV_\perp)^{-1}\partial f_i^0/\partial V_\perp$ for $f_i^0=f_i^0[m_iV_\perp^2/2+\psi(r),v_z]$. The ion orbit integral $\hat{I}$ occurring in Eq. (16) is defined by

$$\hat{I}=i\int_0^{2\pi}\frac{d\phi}{2\pi}\int_{-\infty}^0 d\tau\hat{\phi}(r')\exp[i\ell(\theta'-\theta)-i\omega\tau] \quad , \qquad (17)$$

where the trajectories $r'(\tau)$ and $\theta'(\tau)$ satisfy $r'(\tau=0)=r$ and $\theta'(\tau=0)=\theta$.

B. Eigenvalue Equation for Sharp-Boundary Equilibrium

We now consider the case where the equilibrium ion distribution function is specified by Eq. (10), and the electron and ion density profiles are rectangular [Eq. (11)]. It is evident that the perturbed electron contribution on the right-hand side of Eq. (16) [the term proportional to $\partial n_e^0/\partial r=-n_0\delta(r-R_p)$] is zero except at the surface of the plasma column ($r=R_p$). Moreover, it can be shown that Eq. (16) supports a class of solutions in which the perturbed ion density [the term proportional to $\int d^3V\,V_\perp^{-1}\,\partial f_i^0/\partial V_\perp\ldots$ in Eq. (16)] is also equal to zero except at $r=R_p$. In this case, it follows from the linearized Poisson equation (16) that the electrostatic potential has the simple form $\hat{\phi}(r)=Ar^\ell$ inside the plasma column ($0<r<R_p$), where A is a constant. We substitute $\hat{\phi}(r')=Ar'^\ell$ in Eq. (17) and make use of $[r'\exp(i\theta')]^\ell=[x'+iy']^\ell$, where $x'(\tau)$ and $y'(\tau)$ are

specified by Eq. (14). This readily gives

$$\hat{I}=i(-1)^{\ell}\frac{\hat{\phi}(r)}{\omega_{ci}^{\ell}}\int_{-\infty}^{0}d\tau\exp(-i\omega\tau)[\omega_i\exp(-i\omega_{ci}\tau)-(\omega_i+\omega_{ci})]^{\ell}, \tag{18}$$

where $\hat{\phi}(r)=Ar^{\ell}$. An important feature of Eq. (18) is that the orbit integral $\hat{I}$ is independent of perpendicular energy $m_iV_\perp^2/2$. This is a consequence of the particularly simple form of $\hat{\phi}(r)$ within the plasma column. Finally, after some straightforward algebra that makes use of Eq. (10), the ion velocity integral in Eq. (16) can be carried out to give $\int d^3V\, V_\perp^{-1}\partial f_i^0/\partial V_\perp=(m_iR_p/2\hat{T}_i)\times\partial n_i^0/\partial r=-n_0(m_iR_p/2\hat{T}_i)\delta(r-R_p)$. Substituting into Eq. (16), and making use of $\partial\omega_{pe}^2/\partial r=-\hat{\omega}_{pe}^2\delta(r-R_p)$ where $\hat{\omega}_{pe}^2=4\pi n_0e^2/m_e$, the linearized Poisson equation for perturbations about the sharp-boundary equilibrium described by Eqs. (10) and (11) can be expressed as

$$\begin{aligned}&\frac{1}{r}\frac{\partial}{\partial r}\left[r\left(1-\frac{\omega_{pe}^2(r)}{\omega^2-\omega_{ce}^2}\right)\frac{\partial}{\partial r}\hat{\phi}(r)\right]-\frac{\ell^2}{r^2}\left(1-\frac{\omega_{pe}^2(r)}{\omega^2-\omega_{ce}^2}\right)\hat{\phi}(r)\\&\quad=-\hat{\phi}(r)\left[\frac{\ell}{r}\frac{\omega_{ce}}{\omega}\frac{\hat{\omega}_{pe}^2}{\omega^2-\omega_{ce}^2}+\frac{\hat{\omega}_{pi}^2}{\hat{v}_i^2}R_p\Gamma_{\ell}(\omega)\right]\delta(r-R_p)\ ,\end{aligned} \tag{19}$$

where $\hat{\omega}_{pi}^2=4\pi n_0e^2/m_i$, and $\hat{v}_i^2=2\hat{T}_i/m_i$. The orbit integral $\hat{I}$ [Eq. (18)] occurring in the definition of $\Gamma_{\ell}(\omega)=-1-(\omega-\ell\omega_i)\hat{I}/\hat{\phi}(r)$ can be evaluated explicitly to give

$$\Gamma_{\ell}(\omega)=-1+\left(1+\frac{\omega_i}{\omega_{ci}}\right)^{\ell}\sum_{m=0}^{\ell}\frac{\ell!}{m!(\ell-m)!}\frac{\omega-\ell\omega_i}{\omega+m\omega_{ci}}\left(-\frac{\omega_i}{\omega_i+\omega_{ci}}\right)^{m}\ . \tag{20}$$

In Eq. (20), $\omega_i=\hat{\omega}_i^+$ for a fast rotational equilibrium with axis-encircling orbits, or $\omega_i=\hat{\omega}_i^-$ for a slow rotational equilibrium [Eq. (13)].

C. Dispersion Relation for Sharp-Boundary Equilibrium

The right-hand side of the eigenvalue equation (19) is equal to zero except at the surface of the plasma column ($r=R_p$). Moreover,

since the density is uniform for $0<r<R_p$, and zero for $r>R_p$, the eigenfunction $\hat{\phi}(r)$ satisfies the vacuum Poisson equation $r^{-1}(\partial/\partial r) \times [r\partial\hat{\phi}/\partial r]-(\ell^2/r^2)\hat{\phi}=0$, except at $r=R_p$. Therefore, the solution to Eq. (19) can be expressed as

$$\hat{\phi}_i(r)=Ar^{\ell} \quad , \quad 0\leq r<R_p \quad , \tag{21}$$

inside the column, and

$$\hat{\phi}_0(r)=Ar^{\ell}\,\frac{(1-R_c^{2\ell}/r^{2\ell})}{(1-R_c^{2\ell}/R_p^{2\ell})} \quad , \quad R_p<r\leq R_c \quad , \tag{22}$$

in the outer vacuum region between the surface of the plasma column and the conducting wall ($r=R_c$). Note that $\hat{\phi}(r)$ is continuous at $r=R_p$, and that $\hat{\phi}_0(r=R_c)=0$. The dispersion relation that determines the complex eigenfrequency ω is determined by multiplying Eq. (19) by r and integrating from $R_p(1-\varepsilon)$ to $R_p(1+\varepsilon)$ with $\varepsilon\to 0_+$. This gives

$$\begin{aligned} R_p\left(\frac{\partial\hat{\phi}_0}{\partial r}\right)_{r=R_p} - R_p\left(1-\frac{\hat{\omega}_{pe}^2}{\omega^2-\omega_{ce}^2}\right)\left(\frac{\partial\hat{\phi}_i}{\partial r}\right)_{r=R_p} \\ =-\left(\ell\,\frac{\omega_{ce}}{\omega}\,\frac{\hat{\omega}_{pe}^2}{\omega^2-\omega_{ce}^2}+\frac{\hat{\omega}_{pi}^2R_p^2}{\hat{v}_i^2}\,\Gamma_{\ell}(\omega)\right)\hat{\phi}(r=R_p) \quad . \end{aligned} \tag{23}$$

Substituting Eqs. (21) and (22) into Eq. (23) and rearranging terms gives the desired dispersion relation

$$\frac{1}{1-(R_p/R_c)^{2\ell}}=\frac{\hat{\omega}_{pe}^2}{2\omega(\omega-\omega_{ce})}+\frac{\hat{\omega}_{pi}^2R_p^2}{2\ell\hat{v}_i^2}\,\Gamma_{\ell}(\omega) \quad , \tag{24}$$

where $\Gamma_{\ell}(\omega)$ is defined in Eq. (20).

IV. ANALYSIS OF DISPERSION RELATION

A. Introduction

The dispersion relation (24) is an algebraic equation of order $\ell+2$ for the complex eigenfrequency ω. In this section, we make use of Eq. (24) to investigate stability properties for a broad range of system parameters $\hat{r}_{Li}/R_p$, $\hat{\omega}_i^{\pm}/\omega_{ci}$, etc. For present purposes it is useful to express Eq. (24) in the equivalent form

$$\frac{1}{1-(R_p/R_c)^{2\ell}} = \chi_e(\omega)+\chi_i(\omega), \tag{25}$$

where the effective electron and ion susceptibilities are defined by

$$\chi_e(\omega) = \frac{\hat{\omega}_{pe}^2}{2\omega(\omega-\omega_{ce})}, \tag{26}$$

and

$$\chi_i(\omega) = \frac{\hat{\omega}_{pi}^2 R_p^2}{2\ell\hat{v}_i^2}\Gamma_\ell(\omega), \tag{27}$$

where $\Gamma_\ell(\omega)$ is defined in Eq. (20).

The term $[1-(R_p/R_c)^{2\ell}]^{-1}$ in Eq. (25) includes the vacuum contribution from the linearized Poisson equation (19), as well as the influence of the conducting wall (finite R_c/R_p). In this regard, the conducting wall has a weak stabilizing effect which is most pronounced for small ℓ. For example, for $R_p/R_c=0.75$, we find $[1-(R_p/R_c)^{2\ell}]=0.4375$, 0.9437, 0.9968, for $\ell=1,5,10$, respectively. We therefore examine Eq. (25) for a fixed value of R_p/R_c in the remainder of this section.

In addition, the mirror-drift-cone instability is usually investigated for low-frequency perturbations satisfying $|\omega| \ll \omega_{ce}$. In this case, the electrons are strongly magnetized and the electron

susceptibility can be approximated by

$$\chi_e(\omega) = -\frac{\hat{\omega}_{pe}^2}{2\omega_{ce}\omega} \quad . \tag{28}$$

For $\chi_e(\omega)$ given by Eq. (28), note that the dispersion relation (25) is an algebraic equation of order $\ell+1$ for the complex eigenfrequency ω. For sufficiently low ℓ-values [Secs. IV.B and IV.C], Eq. (28) is a completely adequate approximation for the electron susceptibility $\chi_e(\omega)$. Only for very large ℓ-values is it necessary to use the more accurate expression for $\chi_e(\omega)$ given in Eq. (26) [Sec. IV.D].

Since Eq. (25) is an algebraic equation for ω, several general (but precise) statements can be made regarding the solutions and conditions for instability. We summarize here these general results, before a detailed numerical analysis of Eq. (25). The proof of the following statements is left as an exercise for the reader:

(a) For given ℓ, when instability exists, Eq. (25) permits only <u>one</u> unstable solution with $\mathrm{Im}\omega=\gamma>0$.

(b) For $\ell=1$, the system is stable ($\mathrm{Im}\omega=0$) for both fast ($\omega_i=\hat{\omega}_i^+$) and slow ($\omega_i=\hat{\omega}_i^-$) rotational equilibria.

(c) For $\omega_i=\hat{\omega}_i^+$, the onset of instability occurs for $\ell=2$.

(d) For $\omega_i=\hat{\omega}_i^-$, the system is stable for $\ell < -\omega_{ci}/\hat{\omega}_i^-$. That is, $\mathrm{Im}\omega=0$ for

$$\ell < 2\left[1-\left(1-\frac{4\hat{r}_{Li}^2}{R_p^2}\right)^{1/2}\right]^{-1} \quad . \tag{29}$$

For sufficiently small values of ion Larmor radius that $4\hat{r}_{Li}^2 << R_p^2$, Eq. (29) implies that the system is stable for a substantial range of azimuthal mode numbers satisfying $\ell < R_p^2/\hat{r}_{Li}^2$.

We now examine the detailed stability results predicted by Eq. (25). In Secs. IV.B and IV.C, Eq. (25) is solved numerically for mode numbers $\ell \leq 20$. The two cases, fast rotational equilibria with $\omega_i=\hat{\omega}_i^+$ [Sec. IV.B], and slow rotational equilibria with $\omega_i=\hat{\omega}_i^-$ [Sec. IV.C], are treated separately. In Sec. IV.D, we investigate stability behavior for sufficiently high-frequency perturbations (large ℓ-values) that the ions can be treated as unmagnetized. This leads to a simplified expression for the orbit integral $\hat{I}$ [Eq. (18)] that occurs in the definition of $\Gamma_\ell(\omega)=-1-(\omega-\ell\omega_i)\hat{I}/\hat{\phi}(r)$. Finally, in Sec. IV.E, we investigate the range of validity of the cold-electron approximation.

As a general remark, the reader should keep in mind that the dispersion relation (25) is fully nonlocal, and is valid for the entire allowed range of the equilibrium parameter $2\hat{r}_{Li}/R_p$, i.e., $0 < 2\hat{r}_{Li}/R_p < 1$, as well as for fast rotational equilibria ($\omega_i=\hat{\omega}_i^+$) and slow rotational equilibria ($\omega_i=\hat{\omega}_i^-$).

B. Fast Rotational Equilibrium ($\omega_i=\omega_i^+$)

We first analyse the dispersion relation (25) for the class of fast rotational equilibria with $\omega_i=\hat{\omega}_i^+=-(\omega_{ci}/2)[1+(1-4\hat{r}_{Li}^2/R_p^2)^{1/2}]$. In this case, Eq. (20) reduces to

$$\Gamma_\ell(\omega)=-1+\left(-\frac{\hat{\omega}_i^-}{\omega_{ci}}\right)^\ell \sum_{m=0}^{\ell} \frac{\ell!}{m!(\ell-m)!}\,\frac{\omega-\ell\hat{\omega}_i^+}{\omega+m\omega_{ci}}\left(\frac{\hat{\omega}_i^+}{\hat{\omega}_i^-}\right)^m. \tag{30}$$

Typical numerical results are summarized in Figs. 4 and 5 for $\omega_{pe}^2/\omega_{ce}^2=10$ and $R_p/R_c=0.5$, and azimuthal mode number in the range $2 \leq \ell \leq 20$. Apart from the slight decrease in growth rate for $\ell=4$ and $\hat{r}_{Li}/R_p=0.5$, we note from Fig. 4(a) that the growth rate

$\gamma=\mathrm{Im}\omega$ is a monotonic increasing function of mode number ℓ. Moreover, for each ℓ, the growth rate decreases as $\hat{r}_{Li}/R_p$ is increased. Similarly, from Fig. 4(b), we find that the real oscillation frequency $\omega_r=\mathrm{Re}\omega$ is an increasing function of ℓ, and a decreasing function of $\hat{r}_{Li}/R_p$. This is further illustrated in Fig. 5, where γ/ω_{ci} [Fig. 5(a)] and ω_r/ω_{ci} [Fig. 5(b)] are plotted versus $\hat{r}_{Li}/R_p$ for several values of ℓ. Indeed, for large enough values of ℓ, it is evident from Figs. 4 and 5 that the growth rate γ scales as $\ell^{1/2}$, and the oscillation frequency scales as ℓ. As a general remark, for a fast rotational equilibrium with $\omega_i=\hat{\omega}_i^+$, the growth rate and oscillation frequency tend to exhibit a smooth, monotonic dependence on $\hat{r}_{Li}/R_p$ and mode number ℓ. Moreover, for the sharp-boundary equilibrium considered here, the instability growth rate can be substantial (several times ω_{ci}).

C. Slow Rotational Equilibrium ($\omega_i=\hat{\omega}_i^-$)

We now examine Eq. (25) for the class of slow rotational equilibria with $\omega_i=\hat{\omega}_i^-=-(\omega_{ci}/2)[1-(1-4\hat{r}_{Li}^2/R_p^2)^{1/2}]$. In this case Eq. (20) reduces to

$$\Gamma_\ell(\omega)=-1+\left(-\frac{\hat{\omega}_i^+}{\omega_{ci}}\right)^\ell \sum_{m=0}^{\ell}\frac{\ell!}{m!(\ell-m)!}\frac{\omega-\ell\hat{\omega}_i^-}{\omega+m\omega_{ci}}\left(\frac{\hat{\omega}_i^-}{\hat{\omega}_i^+}\right)^m . \qquad (31)$$

For $4\hat{r}_{Li}^2/R_p^2 \ll 1$, we note that $\hat{\omega}_i^- \simeq -(\hat{r}_{Li}^2/R_p^2)\omega_{ci}=\omega_{di}$, which corresponds to a slow diamagnetic rotation of the ions. On the other hand, for $4\hat{r}_{Li}^2/R_p^2=1$, the rotation frequency $\hat{\omega}_i^-$ reduces to $\hat{\omega}_i^-=-\omega_{ci}/2$ [Fig. 3]. Typical numerical results are summarized in Figs. 6 and 7 for $\hat{\omega}_{pe}^2/\omega_{ce}^2=10$ and $R_p/R_c=0.5$, and azimuthal mode numbers up to $\ell=20$. Figure 6 shows a plot of γ/ω_{ci} [Figs. 6(a)-6(d)] and ω_r/ω_{ci} [Fig. 6(e)] versus mode number ℓ for several values of $\hat{r}_{Li}/R_p$. The real frequency ω_r is plotted in Fig. 6(e) only for the unstable modes with $\gamma>0$.

Several points are noteworthy from Fig. 6. Evidently, the mode structure is far more complicated than in the fast rotational case (Fig. 4). For example, from Figs. 6(a)-6(d), the growth rate γ exhibits an oscillatory dependence on ℓ, although the growth rate, on the average, does increase as a function of ℓ. This is in contrast to Fig. 4, where γ is a monotonic increasing function of ℓ. Moreover, the threshold value of ℓ for instability is a decreasing function of $\hat{r}_{Li}/R_p$ in Fig. 6 [see also Eq. (29)]. For example, for $\hat{r}_{Li}/R_p=0.3$ [Fig. 6(d)] the onset of instability occurs for $\ell=12$, and for $\hat{r}_{Li}/R_p=0.45$ [Fig. 6(a)] the onset of instability occurs for $\ell=4$. This is in contrast to Fig. 4, where the onset of instability always occurs for $\ell=2$. For a specified value of $\hat{r}_{Li}/R_p$, we note from Fig. 6(e) that the oscillation frequency ω_r is an increasing function of ℓ. Figure 7 shows a plot of γ/ω_{ci} [Fig. 7(a)] and ω_r/ω_{ci} [Fig. 7(b)] versus $\hat{r}_{Li}/R_p$ for several values of ℓ. It is evident from Fig. 7(a) that the growth rate γ exhibits an oscillatory dependence on $\hat{r}_{Li}/R_p$. For a specified ℓ, maximum growth tends to occur in the limit of large Larmor radius ($2\hat{r}_{Li}/R_p=1$).

D. High-Frequency Perturbations ($|\omega|>>\omega_{ci}$)

For sufficiently large values of ℓ, it is evident from Secs. IV.B and IV.C that the unstable solution to Eq. (25) satisfies $|\omega|>>\omega_{ci}$. This implies that the ions are essentially unmagnetized on the time scale of the instability. We make use of this fact to obtain a simplified representation of $\Gamma_\ell(\omega)$, valid for large ℓ-values. From Eq. (18) and the definition, $\Gamma_\ell(\omega)=-1-(\omega-\ell\omega_i)\hat{I}/\hat{\phi}(r)$, the quantity $\Gamma_\ell(\omega)$ can be expressed as

$$\Gamma_\ell(\omega)=-1-i(\omega-\ell\omega_i)\frac{(-1)^\ell}{\omega_{ci}^\ell}\int_{-\infty}^{0}d\tau\exp(-i\omega\tau)[\omega_i\exp(-i\omega_{ci}\tau)-(\omega_i+\omega_{ci})]^\ell . \tag{32}$$

Expanding $\exp(-i\omega_{ci}\tau)$ for $\omega_{ci}^2\tau^2 << 1$, we find $[\omega_i\exp(-i\omega_{ci}\tau)-(\omega_i+\omega_{ci})]^\ell = (-1)^\ell\omega_{ci}^\ell[1+i\omega_i\tau+\frac{1}{2}\omega_i\omega_{ci}\tau^2+\ldots]^\ell$. Representing $[1+i\omega_i\tau+\frac{1}{2}\omega_i\omega_{ci}\tau^2+\ldots]^\ell = \exp[\ell\ell n(1+i\omega_i\tau+\frac{1}{2}\omega_i\omega_{ci}\tau^2+\ldots)]\simeq\exp[\ell(i\omega_i\tau+\frac{1}{2}\omega_i\omega_{ci}\tau^2+\frac{1}{2}\omega_i^2\tau^2+\ldots)]$, the expression for $\Gamma_\ell(\omega)$ in Eq. (32) can be approximated by

$$\Gamma_\ell(\omega)=-1-i(\omega-\ell\omega_i)\int_0^\infty d\tau\exp[i(\omega-\ell\omega_i)\tau]\exp\left(-\frac{\ell}{2}\frac{\hat{v}_i^2}{R_p^2}\tau^2\right), \tag{33}$$

where use has been made of the equilibrium constraint $\omega_i(\omega_i+\omega_{ci})=\omega_{di}\omega_{ci}=-\hat{v}_i^2/R_p^2$. We introduce the Z-function representation (for $Im\xi>0$)

$$Z(\xi)=i\int_0^\infty d\tau\exp(i\xi\tau-\tau^2/4)=\frac{1}{\sqrt{\pi}}\int_{-\infty}^{\infty}dx\,\frac{\exp(-x^2)}{x-\xi} . \tag{34}$$

Making use of Eqs. (27), (33), and (34), the effective ion susceptibility for large ℓ-values can be expressed in the convenient form

$$\chi_i(\omega)=-\frac{\hat{\omega}_{pi}^2R_p^2}{2\ell\hat{v}_i^2}[1+\xi Z(\xi)] , \tag{35}$$

where

$$\xi=\frac{(\omega-\ell\omega_i)}{(2\ell\hat{v}_i^2/R_p^2)^{1/2}} . \tag{36}$$

Substituting Eq. (35) into Eq. (25), the dispersion relation reduces to

$$\frac{1}{1-(R_p/R_c)^{2\ell}}=\frac{\hat{\omega}_{pe}^2}{2\omega(\omega-\omega_{ce})}-\frac{\hat{\omega}_{pi}^2R_p^2}{2\ell\hat{v}_i^2}[1+\xi Z(\xi)] , \tag{37}$$

where ξ is defined in Eq. (36).

Equation (37) can be used to investigate stability properties for ℓ-values sufficiently large that $|\omega|>>\omega_{ci}$. As evident from Figs. 4 and 5, this is a particularly easy inequality to satisfy for fast rotational equilibria with $\omega_i=\hat{\omega}_i^+$. In fact, for purposes

of numerical analysis, the Z-function representation of the ion susceptibility in Eq. (37) represents a considerable simplification (for large ℓ-values) over the series representation in Eqs. (30) and (31).

As a simple limiting case, we consider Eq. (37) in the limit where

$$|\xi| = \frac{|\omega-\ell\omega_i|}{(2\ell\hat{v}_i^2/R_p^2)^{1/2}} >> 1 . \tag{38}$$

In this case $1+\xi Z(\xi)\simeq -1/2\xi^2$, and Eq. (37) reduces to

$$\frac{1}{1-(R_p/R_c)^{2\ell}} = \frac{\hat{\omega}_{pe}^2}{2\omega(\omega-\omega_{ce})} + \frac{\hat{\omega}_{pi}^2}{2(\omega-\ell\omega_i)^2} . \tag{39}$$

Equation (39), which is somewhat similar in form to the dispersion relation for the two-stream instability, has been solved numerically for the growth rate $\gamma=\mathrm{Im}\omega$ and real oscillation frequency $\omega_r=\mathrm{Re}\omega$. Typical results are summarized in Fig. 8 where γ/ω_{ci} [Fig. 8(a)] and ω_r/ω_{ci} [Fig. 8(b)] are plotted versus $\ell|\omega_i|/\omega_{ci}$ for hydrogen plasma with $R_p/R_c=0.5$ and $\hat{\omega}_{pe}^2/\omega_{ce}^2=10$. The dashed curves in Fig. 8 are obtained by solving Eq. (39) with the electron susceptibility $\chi_e(\omega)$ approximated by $-\hat{\omega}_{pe}^2/2\omega\omega_{ce}$. Note that this approximation breaks down for $\ell|\omega_i|/\omega_{ci}\gtrsim 2500$ in the plot of oscillation frequency ω_r [Fig. 8(b)], and for $\ell|\omega_i|/\omega_{ci}\gtrsim 400$ in the plot of growth rate γ [Fig. 8(a)]. Note also that the more precise dispersion relation (25) predicts that stabilization ($\gamma=0$) occurs for $\ell|\omega_i|/\omega_{ci}\gtrsim 3800$ (the solid curves in Fig. 8).

A careful examination of Fig. 8 shows that the inequality in Eq. (38) is marginally satisfied for fast rotational equilibria (i.e., $|\xi|\gtrsim 1$ for $\omega_i=\hat{\omega}_i^+$), and is <u>not</u> satisfied for slow rotational equilibria with $\omega_i=\hat{\omega}_i^-$. Therefore, strictly speaking, Eq. (39) should only be used to investigate qualitative features of large-ℓ

stability behavior for fast rotational equilibria. In general, the more precise dispersion relation (37), which includes the plasma dispersion function $Z(\xi)$, can be used to investigate detailed stability properties.

E. Influence of Electron Thermal Effects ($\hat{T}_e \neq 0$)

Throughout the previous sections, the electrons have been treated within the framework of a macroscopic cold-fluid model. Since $\hat{\phi}_i(r)=A(r/R_p)^{\ell}$, for sufficiently large ℓ-values the characteristic half-width of the eigenfunction may easily be comparable with the thermal electron Larmor radius. In this section we make use of a simple kinetic model for the electrons to determine the importance of electron thermal effects. In particular, we assume $f_e^0=(n_0 m_e/2\pi)\times \delta(H_\perp-\omega_e P_\theta-\hat{T}_e)G_e(v_z)$, which is similar in form to the ion distribution function in Eq. (10). This choice of distribution function readily gives a rectangular density profile for $n_e^0(r)$ analogous to Eq. (11), and a parabolic temperature profile $T_{e\perp}^0(r)=\hat{T}_e(1-r^2/R_p^2)$ analogous to Eq. (12). Moreover, it is straightforward to show that $\omega_e(\omega_e-\omega_{ce})=-\omega_{ce}\omega_{de}=-\hat{v}_e^2/R_p^2$, which is simply a statement of equilibrium force balance on an electron fluid element. [Here $\omega_{ce}=eB_0/m_e c$ and $\omega_{de}=(\hat{r}_{Le}^2/R_p^2)\omega_{ce}$.] For present purposes, we assume $\hat{r}_{Le}^2 \ll R_p^2$, and consider a slowly rotating electron equilibrium with

$$\omega_e=\hat{\omega}_e^{-}\simeq\omega_{de}=\frac{r_{Le}^2}{R_p^2}\,\omega_{ce}\,. \tag{40}$$

If we parallel the kinetic stability analysis in Sec. III, treating the electrons in the same manner as the ions, then the electron susceptibility that occurs in the dispersion relation (25) can be expressed as

$$\chi_e(\omega) = \frac{\hat{\omega}_{pe}^2 R_p^2}{2\ell \hat{v}_e^2}\left(1-\frac{\omega_e}{\omega_{ce}}\right)^{\ell}\sum_{m=0}^{\ell}\frac{\ell!}{m!(\ell-m)!}\frac{m\omega_{ce}-\ell\omega_e}{\omega-m\omega_{ce}}\left(\frac{\omega_e}{\omega_{ce}-\omega_e}\right)^m, \tag{41}$$

or equivalently,

$$\chi_e(\omega) = \frac{1}{2\ell}\frac{\hat{\omega}_{pe}^2/\omega_{ce}^2}{\hat{r}_{Le}^2/R_p^2}\left(1-\frac{\hat{r}_{Le}^2}{R_p^2}\right)^{\ell}\sum_{m=0}^{\ell}\frac{\ell!}{m!(\ell-m)!}\frac{m\omega_{ce}-\ell\omega_{ce}\hat{r}_{Le}^2/R_p^2}{\omega-m\omega_{ce}} \times \left(\frac{\hat{r}_{Le}^2/R_p^2}{1-\hat{r}_{Le}^2/R_p^2}\right)^m, \tag{42}$$

where use has been made of Eq. (40). For $|\omega| \lesssim \omega_{ce}$, it is evident from a comparison of Eqs. (26) and (42) that the cold electron response in Eq. (26) is a good approximation to $\chi_e(\omega)$ for azimuthal harmonic numbers satisfying $\ell \lesssim \ell_M$, where $\ell_M \hat{r}_{Le}^2/R_p^2 \sim 1$, or equivalently, $\ell_M(2\hat{r}_{Li}^2/R_p^2)\frac{T_e}{T_i}\frac{m_e}{m_i} \lesssim 1$. As an example, for $2\hat{r}_{Li}^2/R_p^2=1$ (the maximum allowed value), the cold-electron approximation is valid for $\ell \lesssim \ell_M = 1836\ T_i/T_e$.

One of the reasons that the cold-electron approximation is valid for such large ℓ-values in the present analysis is that the <u>local</u> electron temperature (and hence the <u>local</u> electron Larmor radius) is <u>very</u> small near the plasma boundary (where the eigenfunction is highly peaked) for the choice of distribution function $f_e^0=(n_0 m_e/2\pi)\times \delta(H_\perp-\omega_e P_\theta-\hat{T}_e)G_e(v_z)$. This follows since $T_{e\perp}^0(r)=\hat{T}_e(1-r^2/R_p^2)\simeq \hat{T}_e 2\delta r/R_p \ll \hat{T}_e$ for a small distance $\delta r \ll R_p$ from the plasma boundary. Needless to say, if f_e^0 were chosen so that $T_{e\perp}^0(r)$ were approximately uniform over the plasma cross section, then the electrons would provide a stabilizing influence at ℓ-values much smaller than ℓ_M.

V. CONCLUSIONS

In this paper we have made use of a hybrid-kinetic model (Vlasov ions and cold-fluid electrons) to develop a fully nonlocal theory of the mirror-drift-cone instability. After a brief description of equilibrium properties (Sec. II), the electrostatic eigenvalue equation was derived (Sec. III.A) for flute perturbations about a general ion equilibrium $f_i^0(H_\perp-\omega_i P_\theta, v_z)$. In Sec. III.B, we specialized to that particular choice of f_i^0 [Eq. (10)] that gives a rectangular density profile [Eq. (11)] and parabolic temperature profile [Eq. (12)]. The resulting eigenvalue equation [Eq. (19)] was then solved exactly to give a closed algebraic dispersion relation [Eq. (24)] for the complex eigenfrequency ω. Equation (24), which is valid for both slow rotational equilibria ($\omega_i=\hat{\omega}_i^-$) and fast rotational equilibria ($\omega_i=\hat{\omega}_i^+$) with axis encircling orbits, was solved numerically in Sec. IV for a broad range of system parameters. For low ℓ-values (Secs. IV.B and IV.C), the mode structure is macroscopic, and it is found that stability properties are significantly different for $\omega_i=\hat{\omega}_i^+$ (Figs. 4 and 5) and $\omega_i=\hat{\omega}_i^-$ (Figs. 6 and 7). In Sec. IV.D, a simplified form of the dispersion relation was derived for large ℓ-values [Eq. (37)], and finally, in Sec. IV.E, the influence of electron kinetic effects on stability behavior was investigated.

In conclusion, we emphasize that the present sharp-boundary calculation of the mirror-drift-cone instability represents a "worst-case" stability analysis. The stability behavior for diffuse equilibrium profiles is currently under investigation, making use of the hybrid-kinetic eigenvalue equation (16) derived for general $f_i^0(H_\perp-\omega_i P_\theta, v_z)$.

REFERENCES

1. R. F. Post and M. Rosenbluth, Phys. Fluids 9, 730 (1966).
2. D. E. Baldwin, H. L. Berk and L. D. Pearlstein, Phys. Rev. Lett. 36, 1051 (1976).
3. N. T. Gladd and R. C. Davidson, Phys. Fluids 20, 1516 (1977).
4. N. A. Krall, Advances in Plasma Physics (eds. A. Simon and W. B. Thompson, Interscience, New York, 1968), Vol. 1, pp. 153-199.
5. R. E. Aamodt, P. J. Catto, and M. N. Rosenbluth, Bull. Am. Phys. Soc. 23, 755 (1978).
6. R. C. Davidson and H. S. Uhm, Phys. Fluids 21, 60 (1978).
7. R. C. Davidson, Theory of Nonneutral Plasmas (Benjamin, Reading, Mass., 1974).
8. J. P. Freidberg, Phys. Fluids 15, 1102 (1972).
9. R. N. Sudan and M. Rosenbluth, Phys. Rev. Lett. 36, 972 (1976).
10. Y. Shima and T. K. Fowler, Phys. Fluids 8, 2245 (1965).

ACKNOWLEDGMENT

This research was supported by the Department of Energy.

FIGURE CAPTIONS

Fig. 1 Equilibrium configuration and coordinate system.

Fig. 2 Plot of equilibrium density profile [Eq. (11)] and perpendicular temperature profile [Eq. (12)] versus r for choice of ion distribution function in Eq. (10).

Fig. 3 Plot of equilibrium rotation velocities $\hat{\omega}_i^{\pm}$ versus $4\hat{r}_{Li}^2/R_p^2$ [Eq. (13)].

Fig. 4 Plots of (a) normalized growth rate γ/ω_{ci} and (b) real frequency ω_r/ω_{ci} versus harmonic number ℓ for several values of $\hat{r}_{Li}/R_p$ [Eqs. (25) and (30)] and $\omega_i=\hat{\omega}_i^+$.

Fig. 5 Plots of (a) normalized growth rate γ/ω_{ci} and (b) real frequency ω_r/ω_{ci} versus $\hat{r}_{Li}/R_p$ for several values of ℓ [Eqs. (25) and (30)] and $\omega_i=\hat{\omega}_i^+$.

Fig. 6 Plots of (a)-(d) normalized growth rate γ/ω_{ci} and (e) real frequency ω_r/ω_{ci} versus harmonic number ℓ for several values of $\hat{r}_{Li}/R_p$ [Eqs. (25) and (31)] and $\omega_i=\hat{\omega}_i^-$.

Fig. 7 Plots of (a) normalized growth rate γ/ω_{ci} and (b) real frequency ω_r/ω_{ci} versus $\hat{r}_{Li}/R_p$ for several values of ℓ [Eqs. (25) and (31)] and $\omega_i=\hat{\omega}_i^-$.

Fig. 8 Plots of (a) normalized growth rate γ/ω_{ci} and (b) real frequency ω_r/ω_{ci} versus $\ell|\omega_i|/\omega_{ci}$ obtained from Eq. (39) (solid curves). The dashed curves correspond to solving Eq. (39) with $\chi_e(\omega)$ approximated by $-\hat{\omega}_{pe}^2/2\omega\omega_{ce}$.

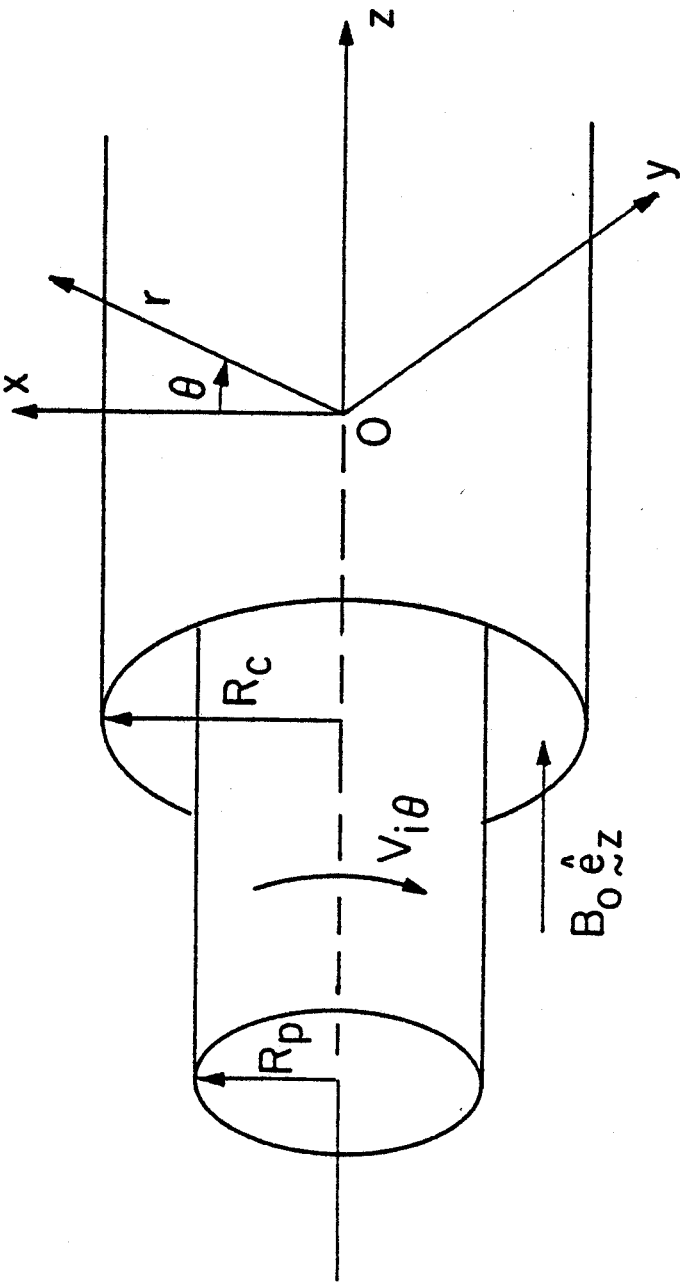

Fig. 1

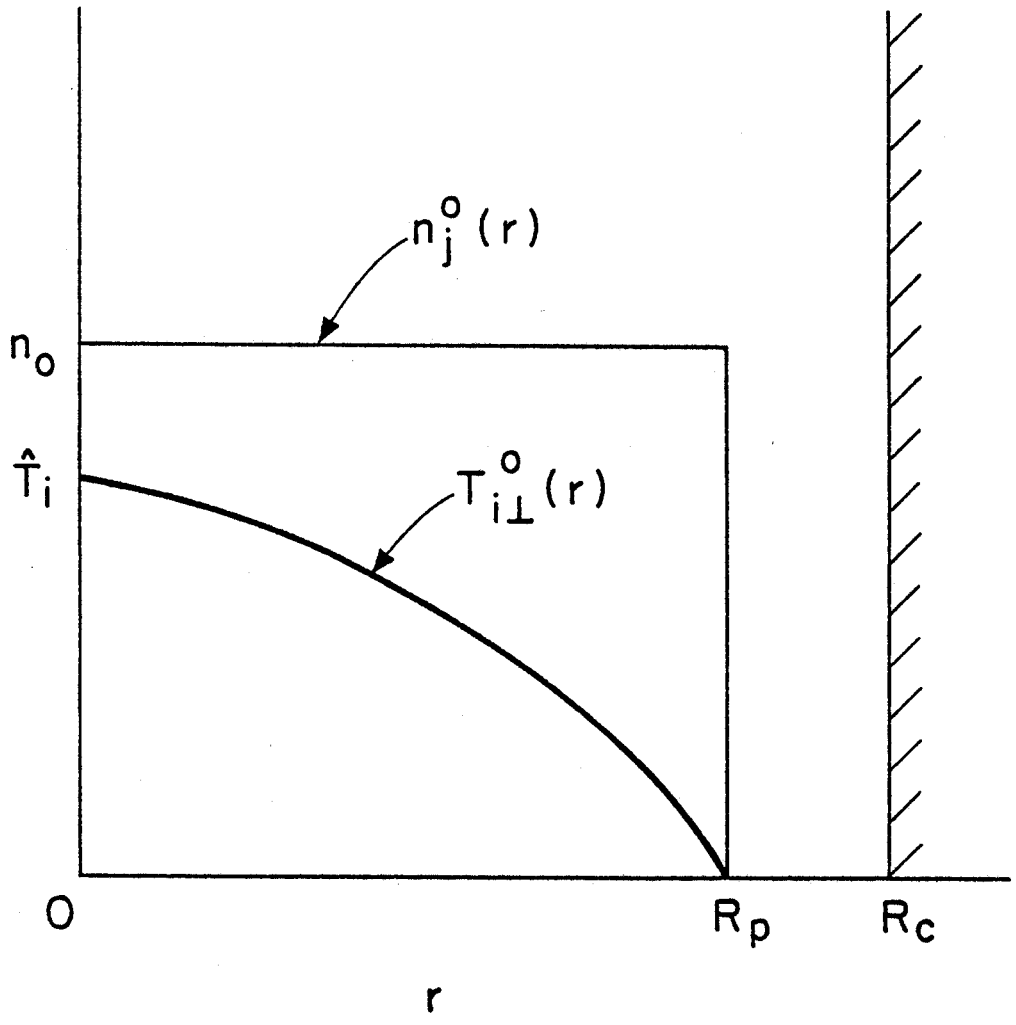

Fig. 2

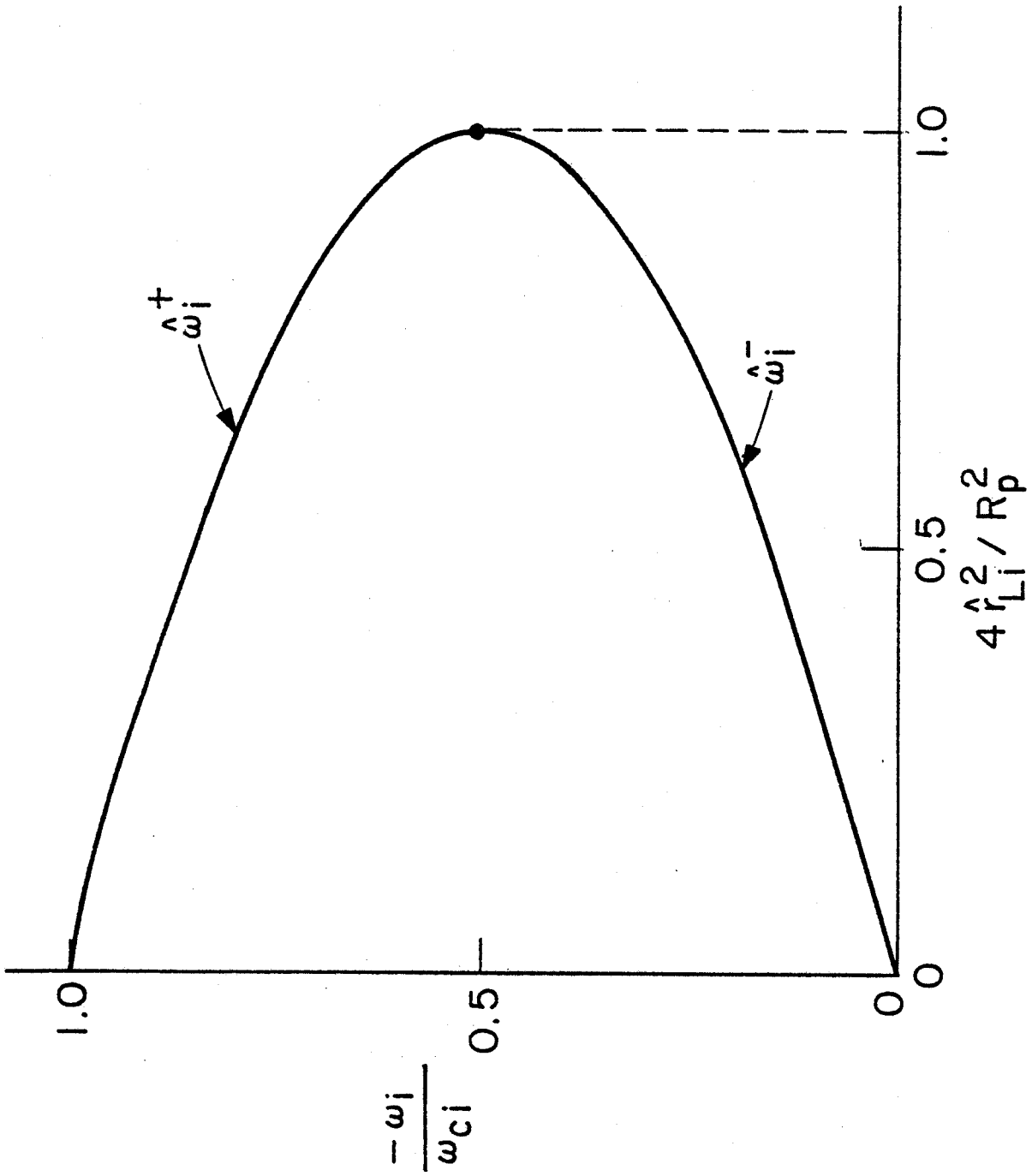
1.0
0.5
0
$\hat{\omega}_i^+$
$\hat{\omega}_i^-$
1.0
0.5
0
$4\hat{r}_{Li}^2 / R_p^2$
$-\frac{\omega_i}{\omega_{ci}}$

Fig. 3

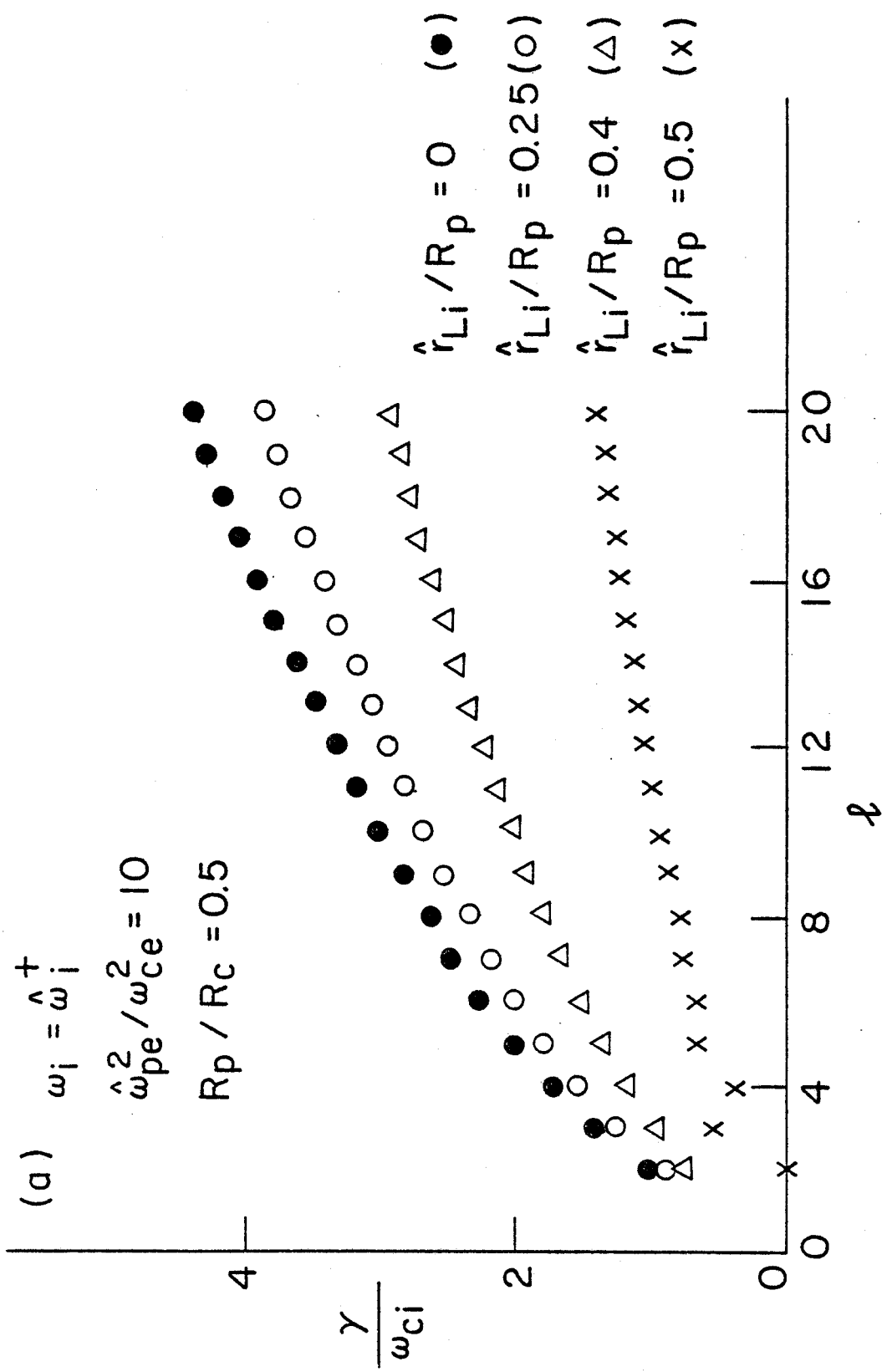
(a)
$\omega_i = \hat{\omega}_i^+$
$\hat{\omega}_{pe}^2/\omega_{ce}^2 = 10$
$R_p / R_c = 0.5$
$\hat{r}_{Li}/R_p = 0$ (●)
$\hat{r}_{Li}/R_p = 0.25$ (○)
$\hat{r}_{Li}/R_p = 0.4$ (△)
$\hat{r}_{Li}/R_p = 0.5$ (×)
$\frac{\gamma}{\omega_{ci}}$
0
2
4
0
4
8
12
16
20
ℓ

Fig. 4(a)

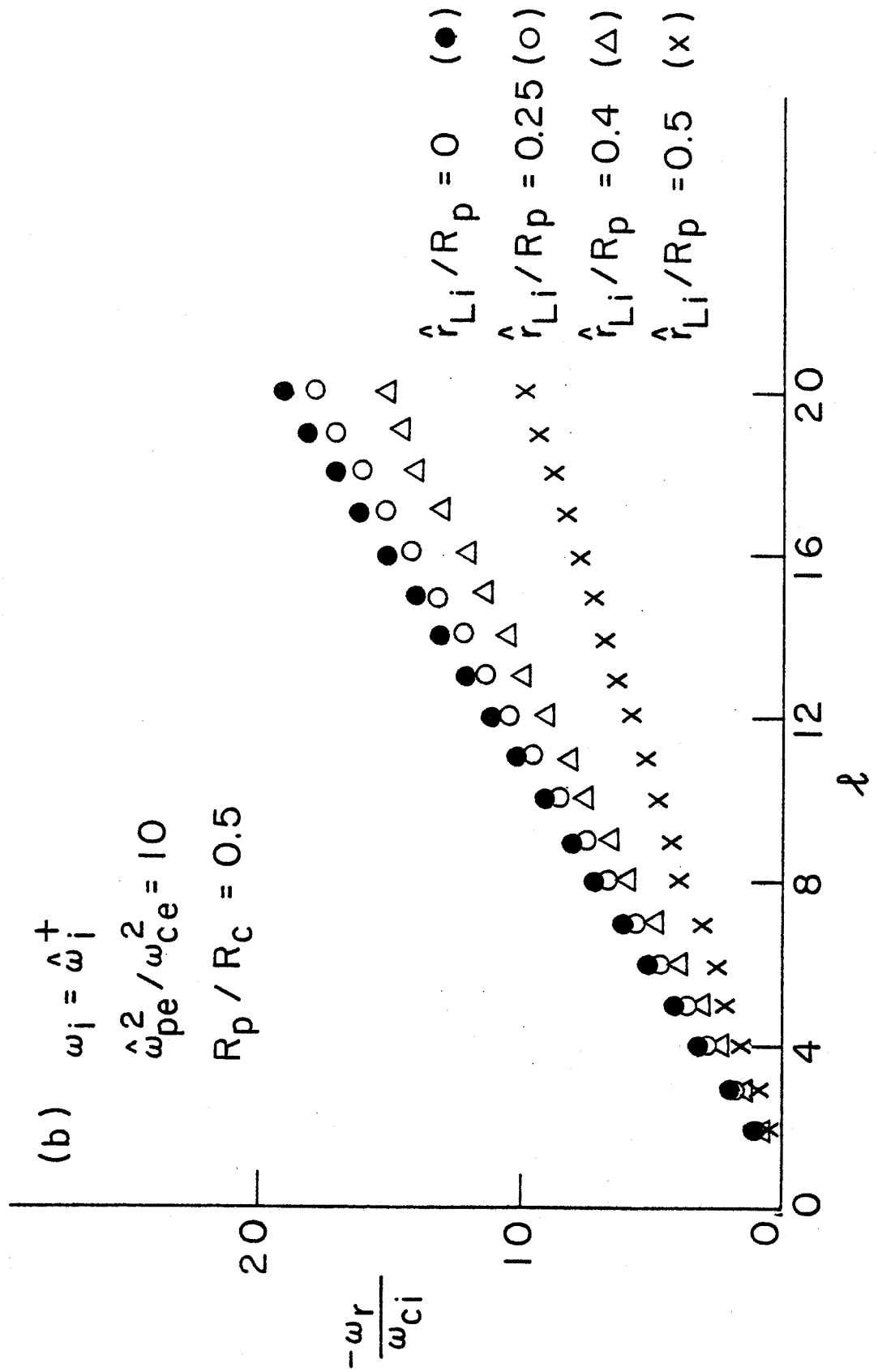
(b)
$\omega_i = \hat{\omega}_i^+$
$\hat{\omega}_{pe}^2/\omega_{ce}^2 = 10$
$R_p / R_c = 0.5$
$\hat{r}_{Li}/R_p = 0$ (●)
$\hat{r}_{Li}/R_p = 0.25$ (○)
$\hat{r}_{Li}/R_p = 0.4$ (△)
$\hat{r}_{Li}/R_p = 0.5$ (×)
$-\frac{\omega_r}{\omega_{ci}}$
20
10
0
0
4
8
12
16
20
ℓ

Fig. 4(b)

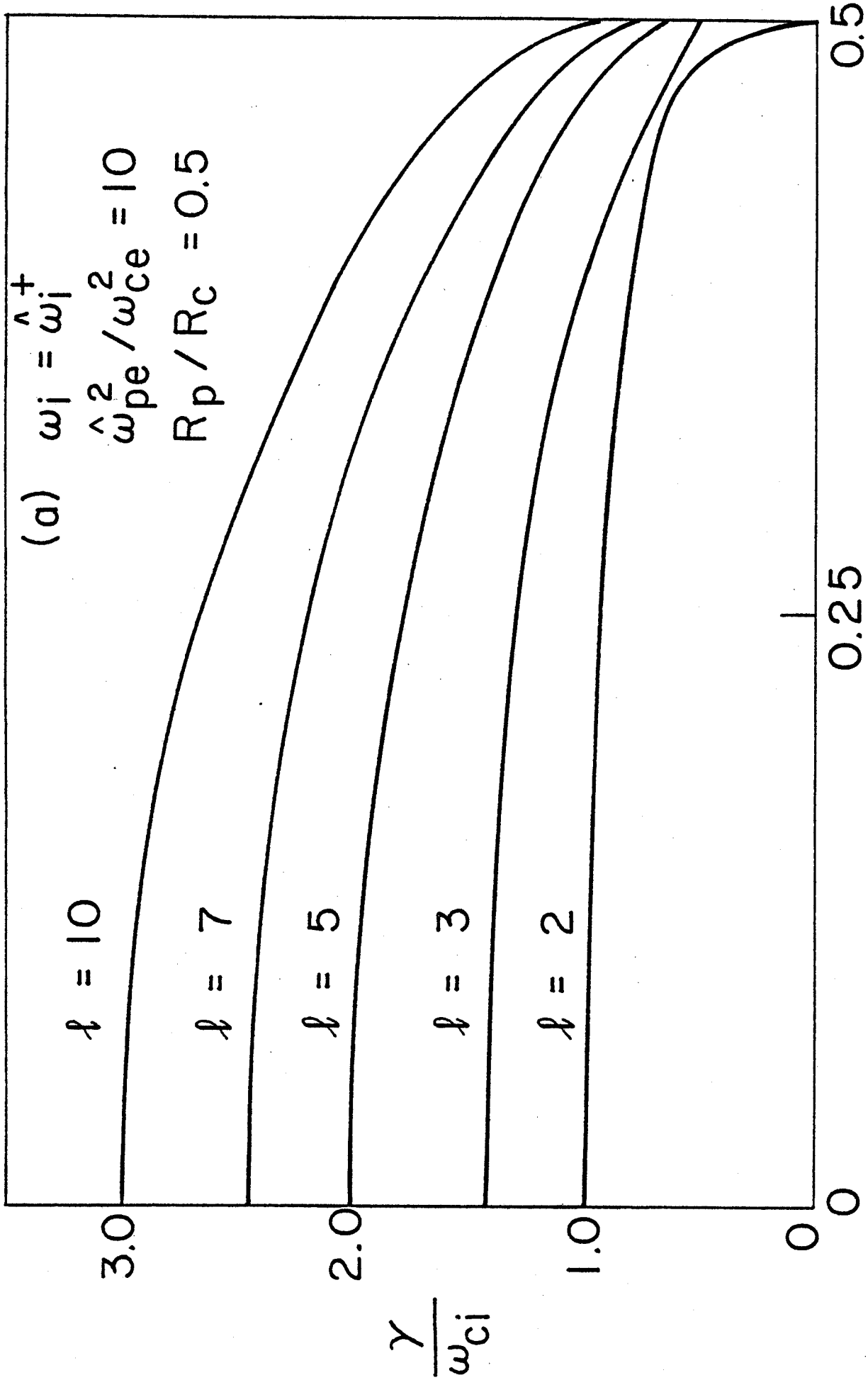
(a) $\omega_i = \hat{\omega}_i^+$
$\hat{\omega}_{pe}^2/\omega_{ce}^2 = 10$
$R_p/R_c = 0.5$
$\ell = 10$
$\ell = 7$
$\ell = 5$
$\ell = 3$
$\ell = 2$
3.0
2.0
1.0
0
$\frac{\gamma}{\omega_{ci}}$
0
0.25
0.5
$\hat{r}_{Li}/R_p$

Fig. 5(a)

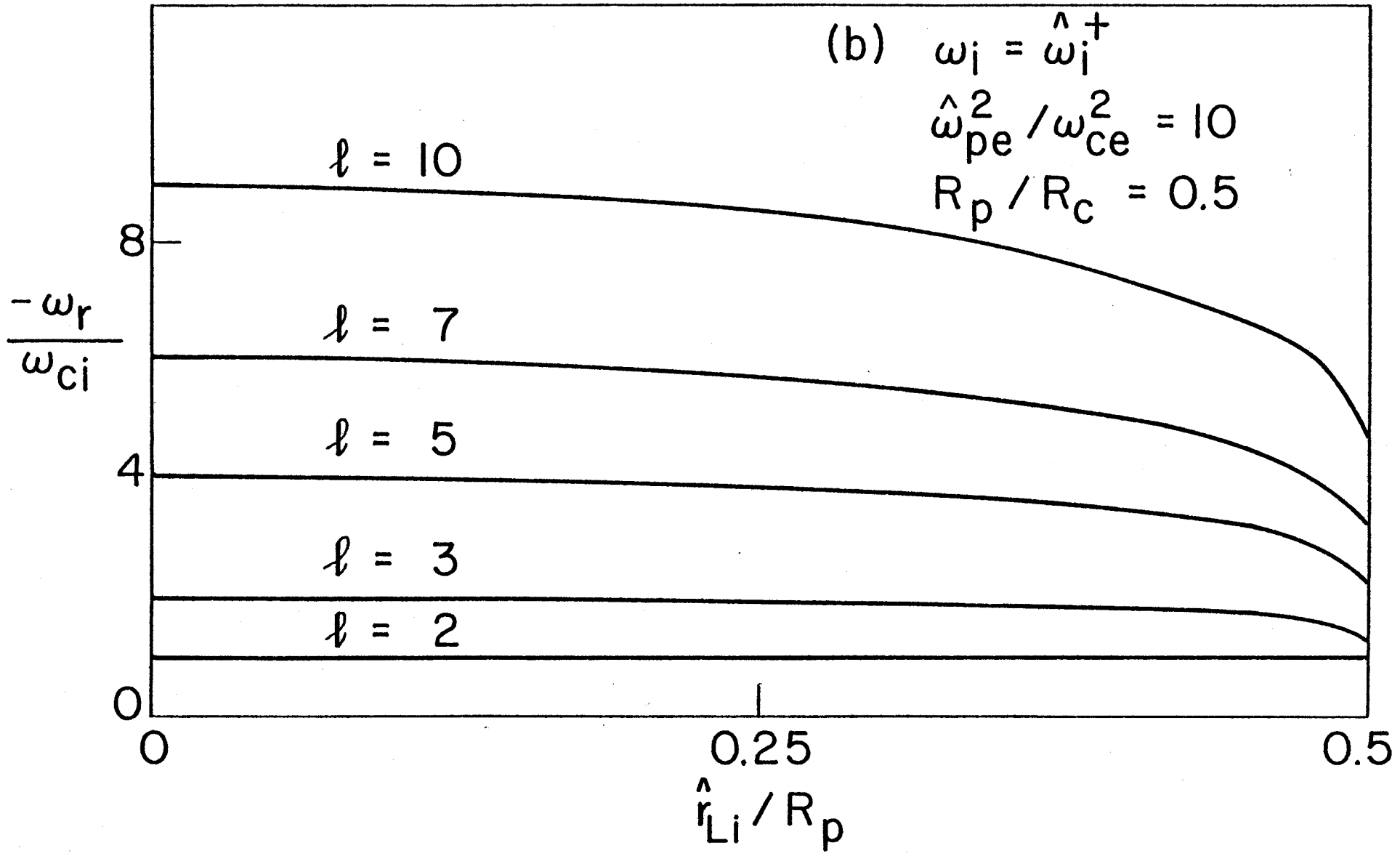
(b) $\omega_i = \hat{\omega}_i^+$
$\hat{\omega}_{pe}^2 / \omega_{ce}^2 = 10$
$R_p / R_c = 0.5$
$\ell = 10$
$\ell = 7$
$\ell = 5$
$\ell = 3$
$\ell = 2$
$\frac{-\omega_r}{\omega_{ci}}$
8
4
0
0
0.25
0.5
$\hat{r}_{Li} / R_p$

Fig. 5(b)

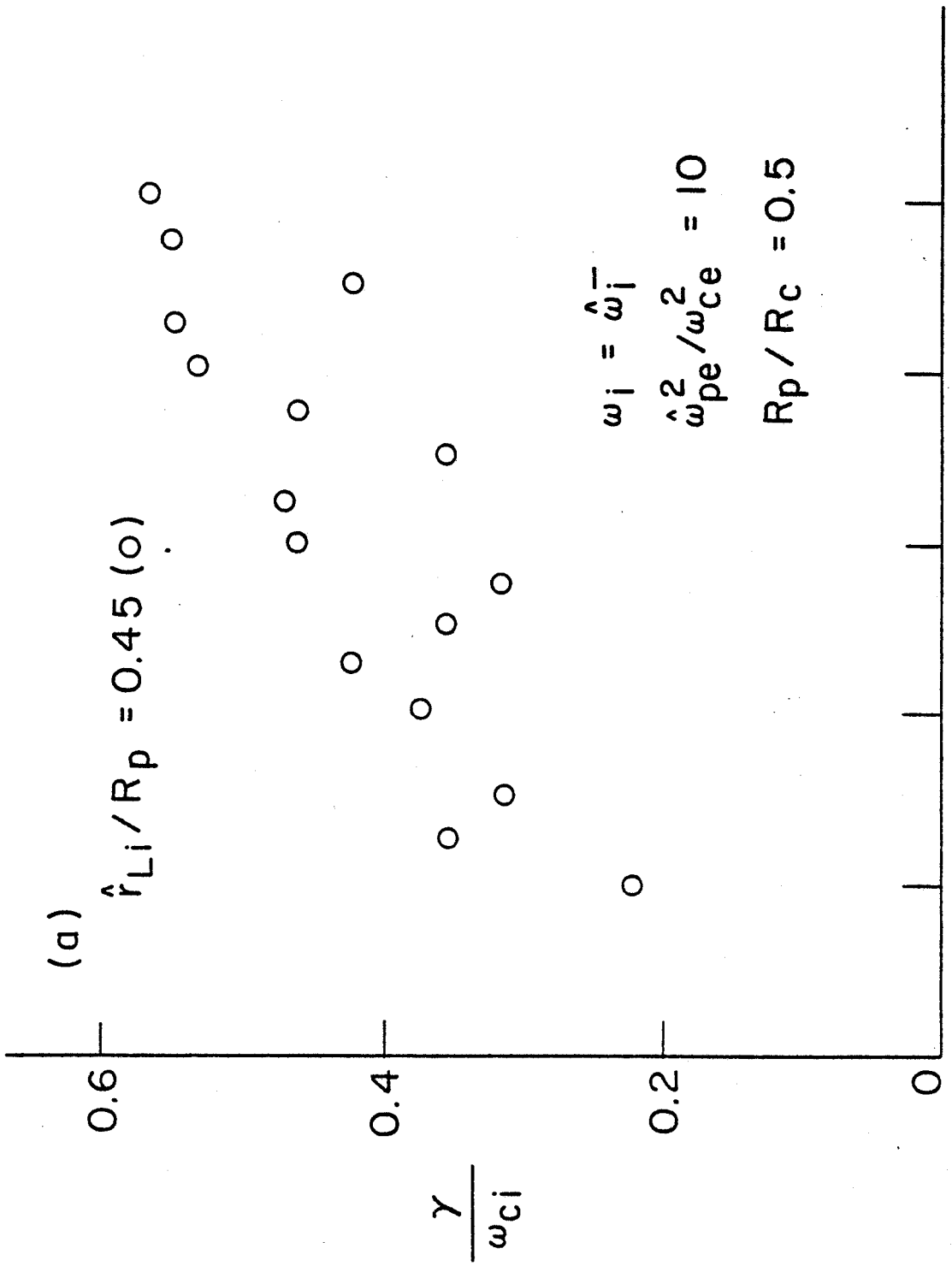
(a)
$\hat{r}_{Li}/R_p = 0.45$ (o)
$\omega_i = \hat{\omega}_i$
$\hat{\omega}_{pe}^2/\omega_{ce}^2 = 10$
$R_p/R_c = 0.5$
$\frac{\gamma}{\omega_{ci}}$
0.6
0.4
0.2
0
0
4
8
12
16
20
ℓ

Fig. 6(a)

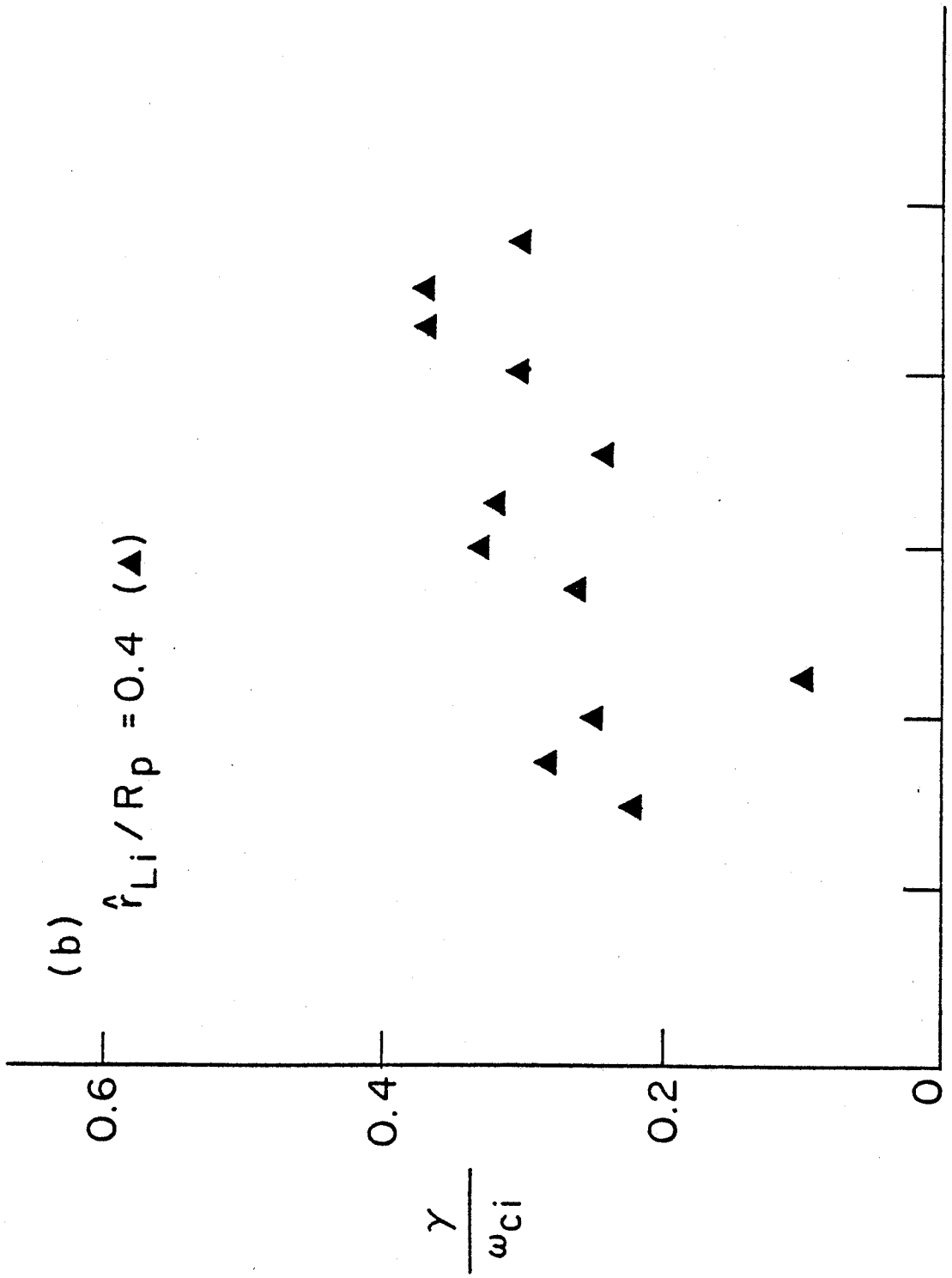

Fig. 6(b)

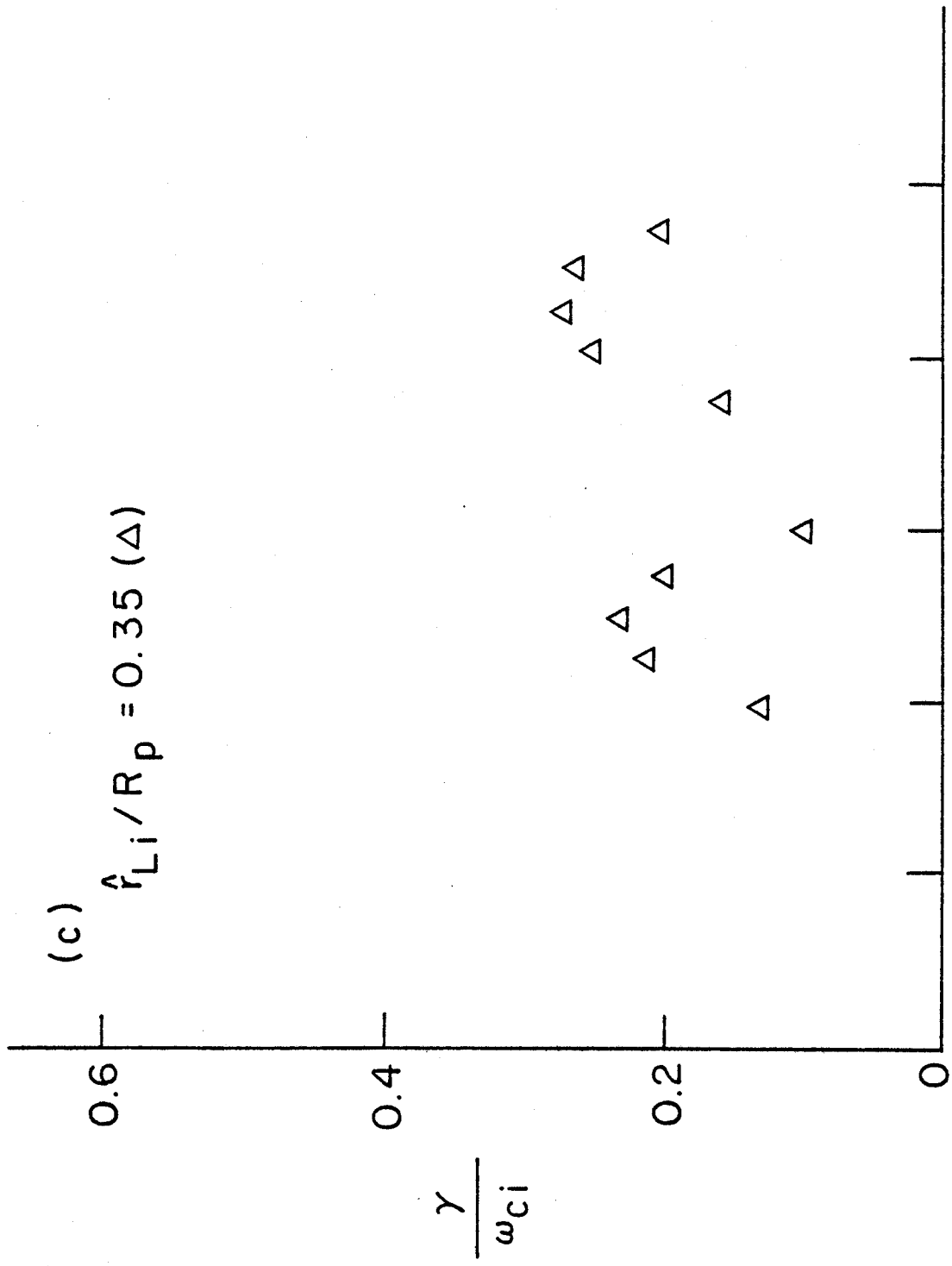

Fig. 6(c)

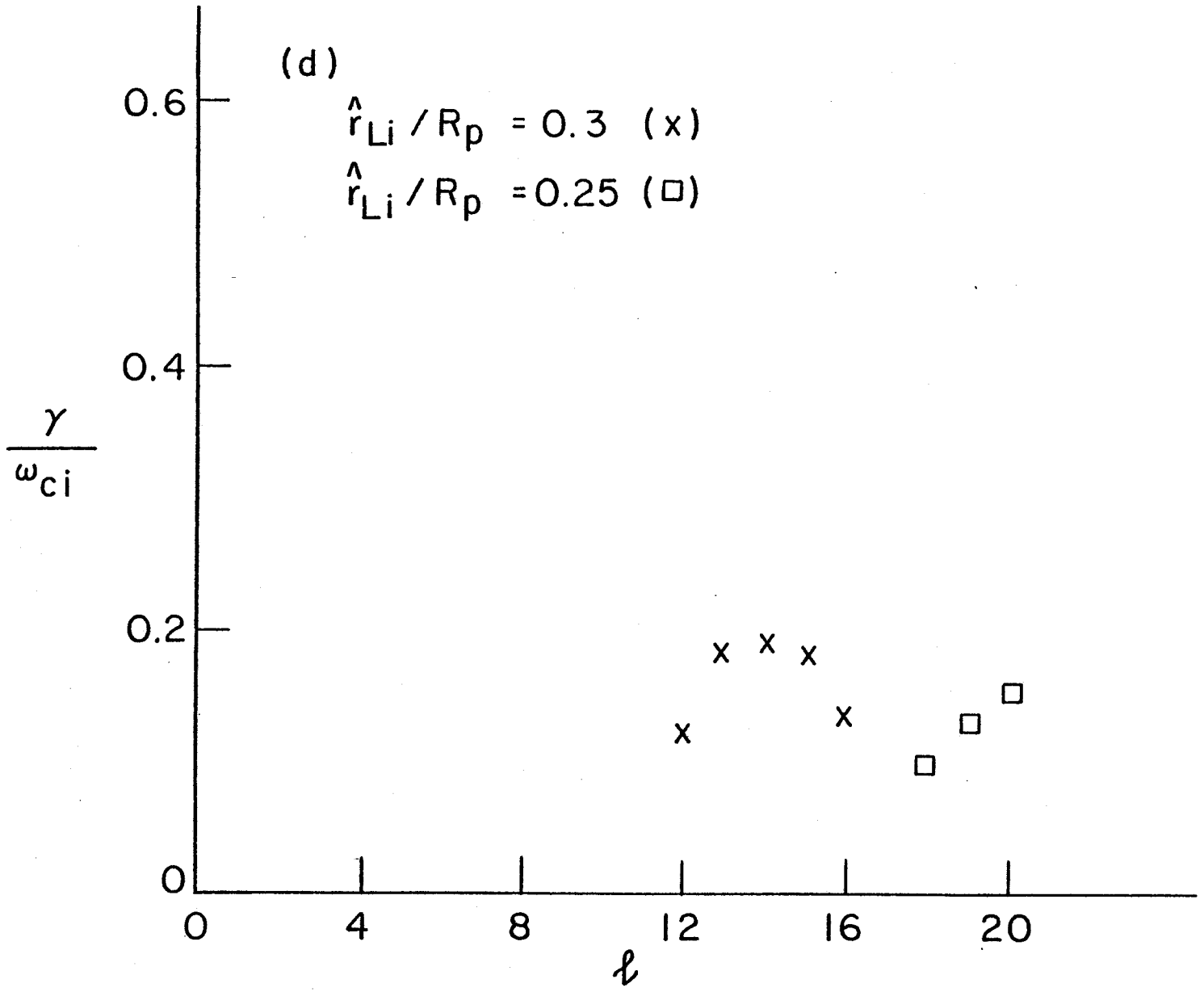
(d)
$\hat{r}_{Li}/R_p = 0.3$ (x)
$\hat{r}_{Li}/R_p = 0.25$ (□)
0.6
0.4
0.2
0
$\frac{\gamma}{\omega_{ci}}$
0
4
8
12
16
20
ℓ

Fig. 6(d)

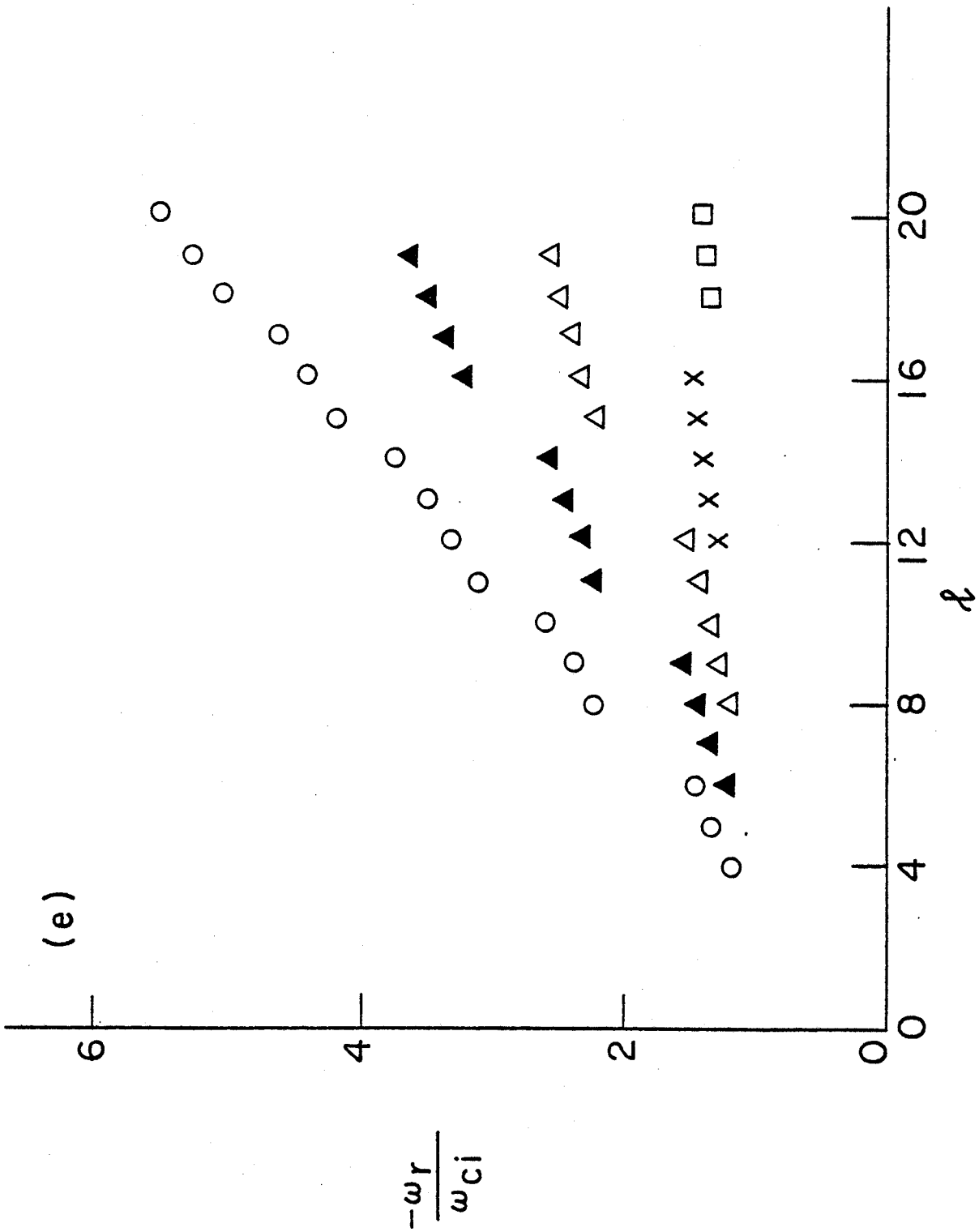

Fig. 6(e)

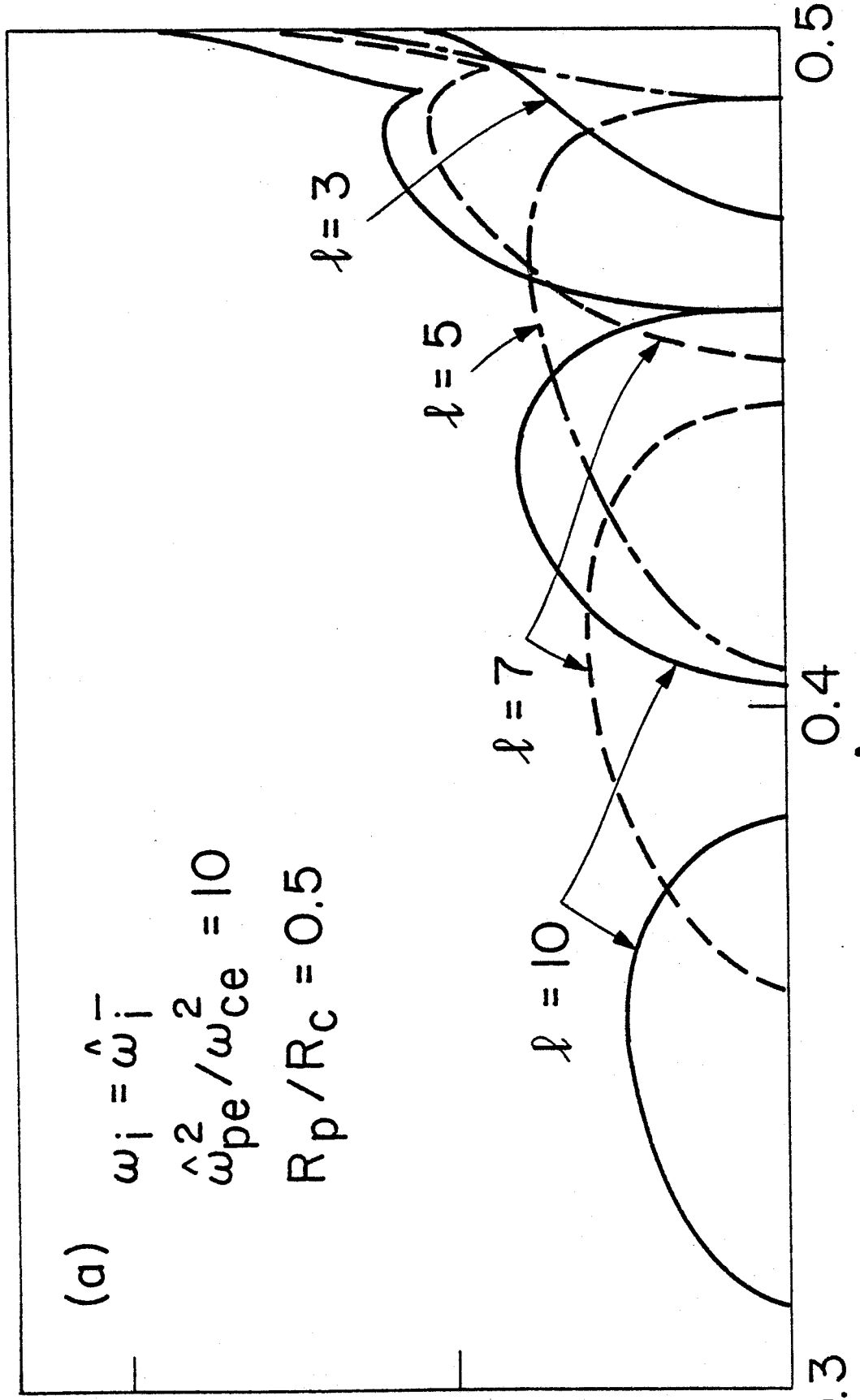
(a)
$\omega_i = \hat{\omega}_i$
$\hat{\omega}^2_{pe}/\omega^2_{ce} = 10$
$R_p/R_c = 0.5$
$\ell = 3$
$\ell = 5$
$\ell = 7$
$\ell = 10$
$\frac{\gamma}{\nu_{ci}}$
1.0
0.5
0.3
0.4
0.5
$\hat{r}_{Li}/R_p$

Fig. 7(a)

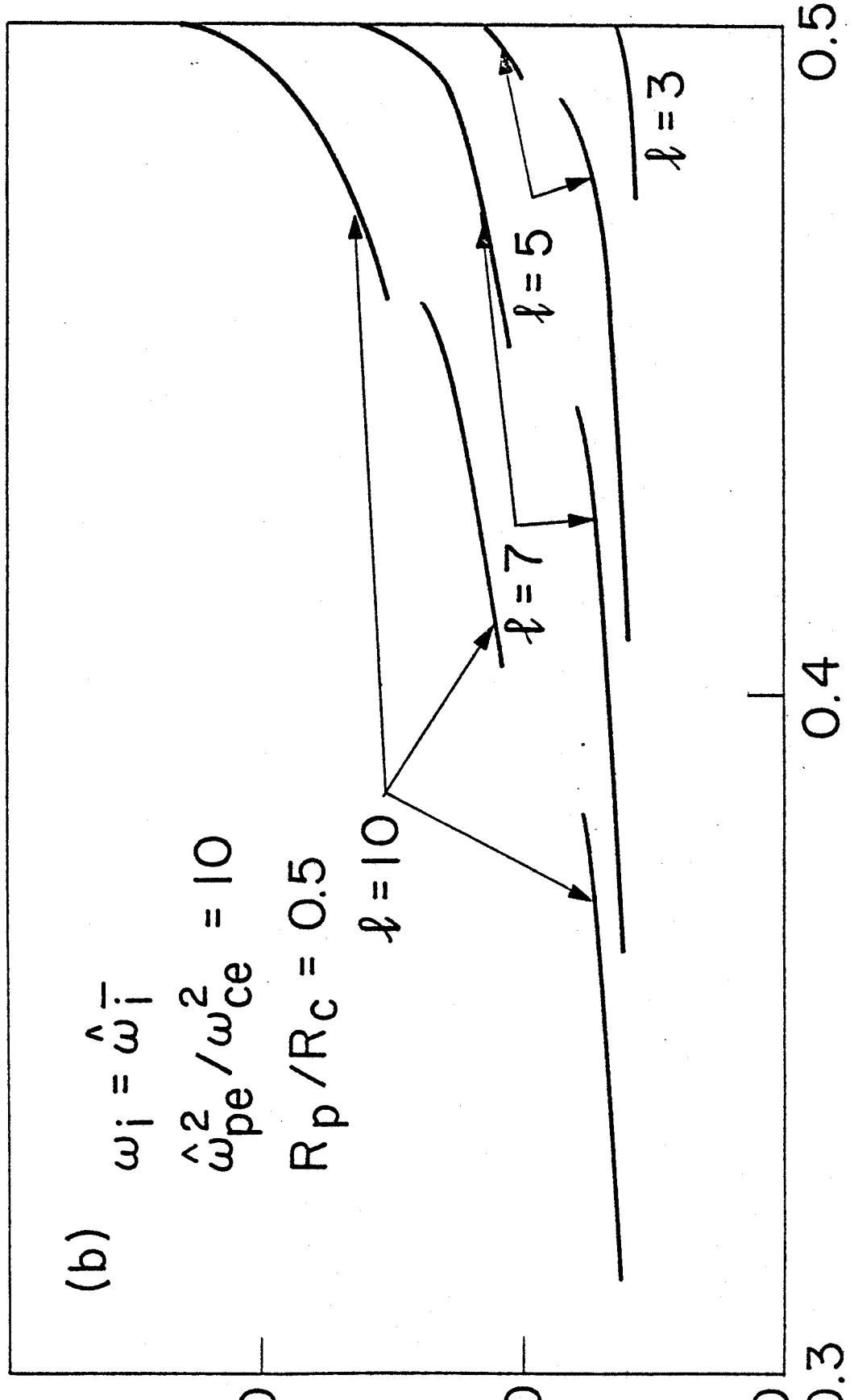
(b)
$\omega_j = \hat{\omega}_j$
$\hat{\omega}_{pe}^2/\omega_{ce}^2 = 10$
$R_p/R_c = 0.5$
$\ell = 10$
$\ell = 7$
$\ell = 5$
$\ell = 3$
$-\frac{\omega_r}{\omega_{ci}}$
4.0
2.0
0
0.3
0.4
0.5
$\hat{r}_{Li}/R_p$

Fig. 7(b)

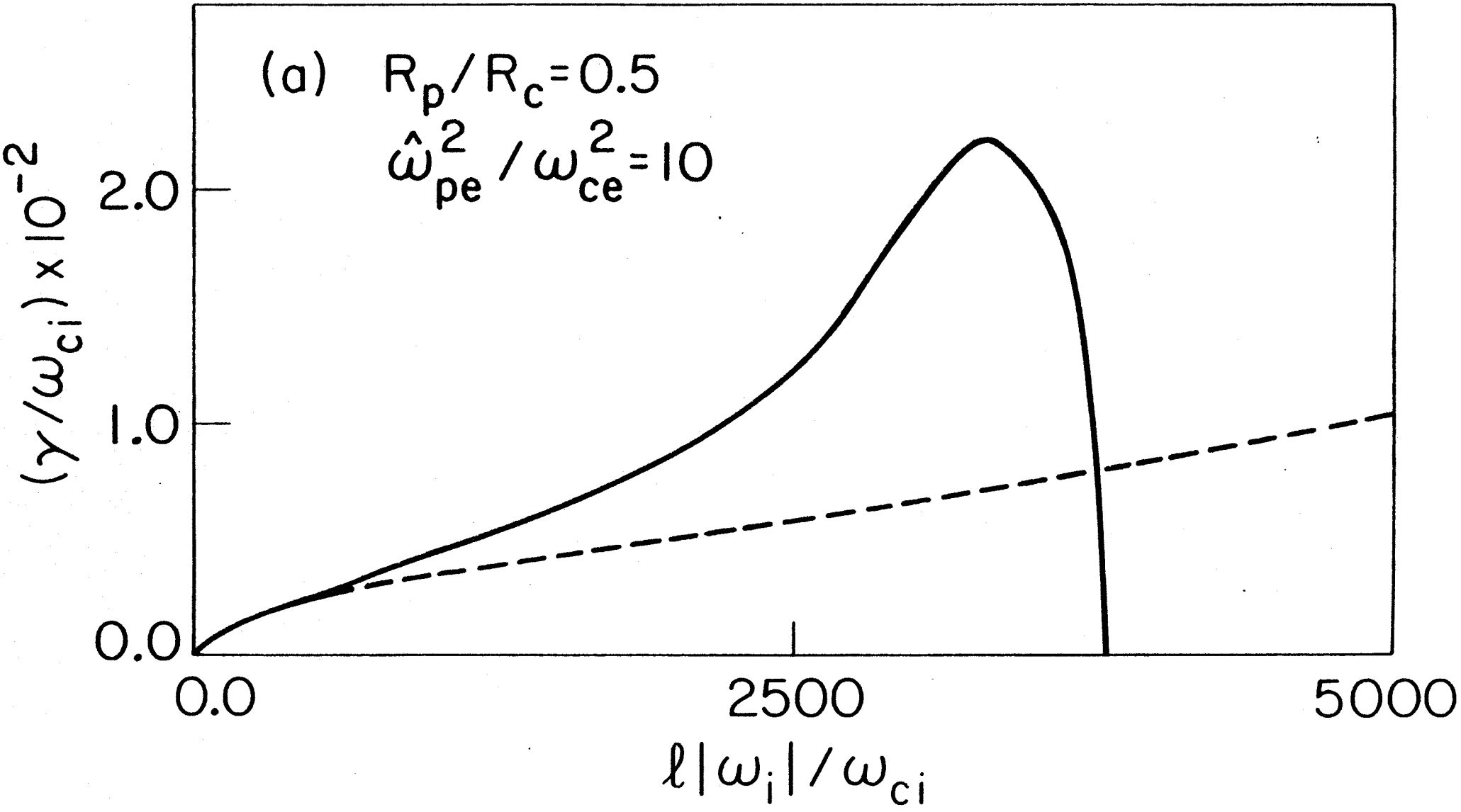
(a) $R_p/R_c=0.5$
$\hat{\omega}_{pe}^2/\omega_{ce}^2=10$
$(\gamma/\omega_{ci}) \times 10^{-2}$
2.0
1.0
0.0
0.0
2500
5000
$\ell|\omega_i|/\omega_{ci}$

Fig. 8(a)

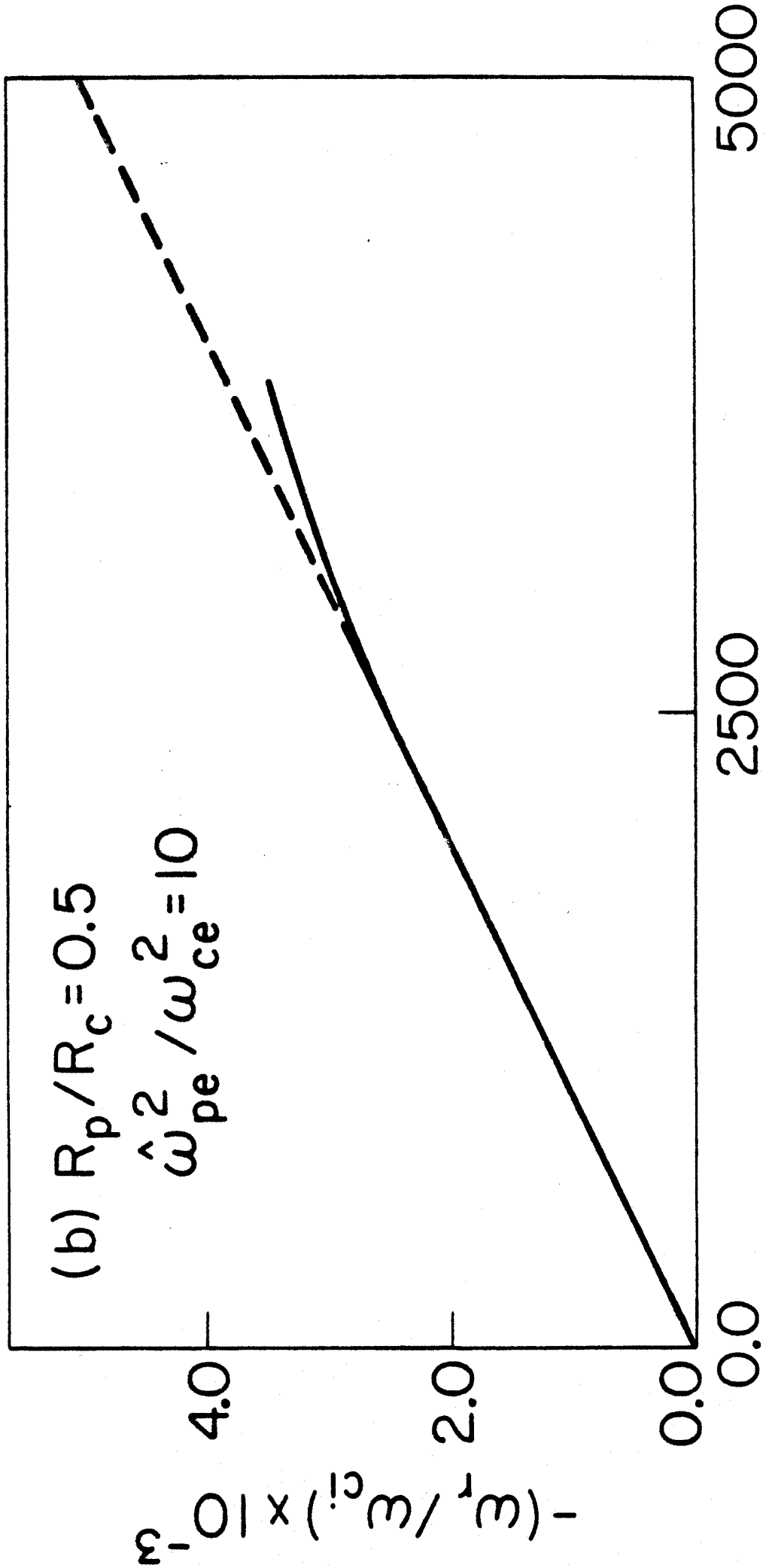
(b) $R_p/R_c=0.5$
$\hat{\omega}^2_{pe}/\omega^2_{ce}=10$
$-(\omega_r/\omega_{ci})\times 10^{-3}$
4.0
2.0
0.0
0.0
2500
5000
$\ell\,|\omega_i|/\omega_{ci}$

Fig. 8(b)